1987

Magnetism in BCC and FCC Manganese.

Gonzalo Fuster
Louisiana State University and Agricultural & Mechanical College

Order Number 8811406

Magnetism in BCC and FCC manganese

Fuster, Gonzalo, Ph.D.

The Louisiana State University and Agricultural and Mechanical Col., 1987

U·M·I
300 N. Zeeb Rd.
Ann Arbor, MI 48106

MAGNETISM IN BCC AND FCC MANGANESE

A Dissertation

Submitted to the Graduate Faculty of the
Louisiana State University and
Agricultural and Mechanical College
in partial fulfillment of the
requirements for the degree of
Doctor of Philosophy

in

The Department of Physics and Astronomy

by

Gonzalo Fuster
B.S., Universidad Católica Valparaíso, Chile, 1978
M.S., Louisiana State University, Baton Rouge, Louisiana, USA, 1985
December 1987

TO MY PARENTS

A MIS PADRES

ACKNOWLEDGMENTS

I wish to express my deep gratitude to Professor Joseph Callaway for his guidance and supervision throughout this research.

The work for this dissertation was done in collaboration with Dr. Nathan Brener, whom I thank for his help and continuous encouragement. I am grateful to Dr. Diola Bagayoko for introducing me to the computer operating system and teaching me the essentials of BNDPKG.

Many thanks are also due to the Physics Department and all its members for good will and help throughout all my graduate studies.

I am grateful to the LSU SNCC for providing excellent technical services in computation, to Norma Duffy for the excellent drawings, and to Ophelia Dudley for the flawless typing of this dissertation.

I acknowledge the support of Universidad Santa Maria, Valparaiso, Chile; LSU Physics Department in the form of a research assistantship on the fall of 1983, spring of 1984 and fall of 1987, and a teaching assistantship for the rest of my stay at L.S.U.

TABLE OF CONTENTS

LIST OF TABLES

LIST OF FIGURES

ABSTRACT

The electronic band structure, magnetic moment, and density of states of bcc and fcc manganese are calculated as a function of the lattice constant, using the LCGO method, on the local density approximation.

For bcc manganese, two magnetic phases were found: a low moment state ($m \simeq 1\ \mu_B$) and a high moment state ($m \geq 2.4\ \mu_B$). For a small range of lattice constants (a = 5.9 to 6.025 a.u.), two local minima of the energy can coexist, yielding two different values of the moment for the same lattice constant.

For fcc manganese, two phases were found: a zero moment state for a less than about 7.25 a.u. and a high moment state ($m \geq 1.88\ \mu_B$).

Both phase transitions are described in detail in terms of the band structure.

CHAPTER 1

INTRODUCTION

The 3d-transition metals (Sc to Ni) present interesting properties with respect to their crystal structures and magnetic phases. Several of them exist in a number of allotropic modifications, like iron (three modifications), cobalt (two), and remarkably, manganese, which exists in four different forms. With respect to their magnetic properties, the transition metals include iron, cobalt, and nickel, which are ferromagnetic, and the antiferromagnetic chromium and manganese.[1] A significant effort has been made to describe theoretically the properties of the transition metals, and the problem is still the object of active research.

The key to the understanding of such a variety of behaviors is the presence of partially filled 3d-bands, which generate complicated Fermi surfaces and density-of-states profiles rich in structures (high peaks and deep valleys), in the region around the Fermi energy. This behavior can be contrasted with that of Cu and Zn, in which the d-bands are totally occupied and the density-of-states curve is totally flat at the Fermi energy.[2]

The above discussion about the peculiar character of the d-bands in the transition metals should make clear that the properties of this group of metals are particularly sensitive to changes in the atomic volume (or, equivalently, the lattice constant).

Several techniques can be used to vary the atomic volume of a

given metal. For example, pressure can be applied to a sample, achieving a contraction of the lattice constant, or the metal can be alloyed with other materials and the properties of the resulting alloy can be studied as a function of the concentration of the metal. Recently, the technique of epitaxial growth has revealed itself to be very promising in the study of expanded lattices and, more remarkably, in the generation of new artificial phases of transition metals.

As an example, body-centered cubic (bcc) cobalt has been synthesized by Walmsley et al.[45] by deposition of compositionally modulated thin films of Co and Cr on a number of substrates and by Prinz[5] by epitaxial growth on a GaAs substrate. Both experiments showed that bcc Co is ferromagnetic. In the first of them, the lattice constant was measured to be 5.234 a.u. and the magnetic moment was found to be very close to that of the hcp phase, namely, $m \simeq 1.71\ \mu_B$. On the other hand, the lattice constant measured in the experiment by Prinz was 5.342 a.u. and the magnetic moment was found to be $1.53\ \mu_B$.

Bagayoko and coworkers[43] calculated the band structure of bcc Co by using the linear combination of gaussian orbitals (LCGO) method[28] for a number of lattice constants in the range of a = 5.0 to 5.45 a.u. The calculated magnetic moment for a = 5.234 a.u. was 1.65 a.u., in good agreement with the experimental value of Walmsley et al. For a = 5.342 a.u., the calculated moment was approximately $1.69\ \mu_B$, which is about 10% larger than the experimental value of

Prinz.

Theoretical calculations of the electronic band structure of transition metals as a function of the lattice constant can be used to predict the existence of metastable phases and the arising of magnetic phase transitions with variations in the atomic volume. A number of calculations of this type can be found in the literature.[7,8,9,10] For example, Bagayoko and Callaway[7] presented a study of the dependence of the magnetic moment on the lattice constant for bcc and face-centered cubic (fcc) iron by using the LCGO method. They found that the magnetic moment increases rather smoothly with the lattice constant for bcc iron. For fcc iron, however, the magnetic moment increases abruptly at a Wigner-Seitz radius of about 2.7 a.u. This feature was identified with the transition from a low-spin to a high-spin ferromagnetic state, which was first described by Madsen and Andersen.[11]

Kübler has employed the 'augmented-spherical-wave' (ASW) method[44] to calculate the total energy for the nonmagnetic, ferromagnetic, and antiferromagnetic phases of several materials, including transition metals such as iron, chromium, and manganese, and some alloys.[8,12,13,14] This approach to the problem is more complete, in the sense that it allows the prediction of which magnetic ordering, either paramagnetic, ferromagnetic, or antiferromagnetic, yields the minimum total energy for a given lattice constant.

Moruzzi and coworkers[9] investigated the magnetic phases of a

number of transition metals by using the ASW method in a different formalism. In their study, both the lattice constant and the magnetic moment are considered parameters of the theory, and the total energy is then calculated for a number of values of the lattice constant and magnetic moment, yielding what they call a 'binding surface.' In this kind of formulation, the ground state corresponds to a minimum with respect to both the lattice constant and the magnetic moment. As an example of the results obtained, they determined the ground state of bcc iron to be ferromagnetic with a Wigner-Seitz radius of r_s = 2.62 a.u. and a magnetic moment of 2.15 μ_B, in good agreement with the experimental values (2.66 a.u. and 2.12 μ_B respectively).[42] For fcc iron, they found the ground state to be paramagnetic with r_s = 2.54 a.u. They also found two local minima, corresponding to low-spin and high-spin metastable ferromagnetic states.

In the present work, we have investigated the electronic band structure and magnetic moment of bcc and fcc manganese as a function of the lattice constant.

Manganese exists in four allotropic modifications (α,β,γ and δ-Mn).[15] At room temperature manganese has a complex cubic structure with 29 atoms per unit cell (α-Mn). This phase becomes antiferromagnetic below 85 K. Over 973 K another complex cubic structure arises, with 20 atoms per unit cell (β-Mn). Between 1350 and 1415 K, the structure is fcc (γ-Mn). This form can be stabilized at room temperature by quenching, yielding a tetragonal

structure. Finally, between 1415 K and the melting point, the structure is bcc (δ-Mn). As far as we know, only one calculation of the electronic band structure of α-Mn has been reported, namely the one by Sasaki and coworkers.[16] They did a tight-binding calculation, based on a Hubbard-like Hamiltonian, for the antiferromagnetic phase of α-Mn.

Several calculations of the electronic band structure of fcc manganese (γ-Mn) have been done for the paramagnetic[4,9,17,42] and for the antiferromagnetic[18,19] states.

Recently, Arrott[6] succeeded in growing bcc Mn on a (100) Fe substrate. While Arrott did not detect ferromagnetism in the bcc Mn layer at this particular lattice constant, his work demonstrates that bcc Mn can be stabilized at room temperature and below by epitaxial growth and suggests that layers of bcc Mn could be produced at other lattice constants by appropriate choice of substrates. The question then arises as to how the magnetic structure of bcc Mn depends on lattice constant. In particular, it would be interesting to investigate whether bcc Mn, and also fcc Mn, have a range of lattice constants in which ferromagnetism would be expected to occur at low temperature.

The problem has been considered by Goodenough,[20] whose work suggested that bcc Mn is antiferromagnetic, and more recently by Kübler.[8,12] Thus, in Ref. 8, Kübler used the ASW method to calculate the electronic band structure and total energy of bcc and fcc manganese for the paramagnetic, ferromagnetic, and antiferromagnetic

states as a function of the Wigner-Seitz radius. Two different antiferromagnetic structures were considered for the fcc case. He found the ground state of fcc Mn to be antiferromagnetic, with planes of alternating up and down spins parallel to the (001) plane and Wigner-Seitz radius of about 2.6 a.u. In addition, he found this antiferromagnetic phase to be the state of minimum energy for the whole range of Wigner-Seitz radii considered ($r_s \approx 2.55$ to 2.85 a.u.)

On the other hand, for bcc Mn he found the ground state to be ferromagnetic with a Wigner-Seitz radius of 2.6 a.u. and a magnetic moment of about $0.6\mu_B$. This ferromagnetic phase is the state of minimum energy up to a Wigner-Seitz radius of about 2.73 a.u. At this point the antiferromagnetic phase becomes the state of minimum energy, indicating a phase transition from ferromagnetism to antiferromagnetism.

In the present work, we have used the linear combination of gaussian orbitals (LCGO) method to perform a spin-polarized calculation of the energy bands, magnetic moment, and density of states of bcc and fcc Mn for a number of lattice constants.

The results for bcc Mn were reported in Ref. 10. We found an abrupt transition from a low moment to a high moment magnetic state at some lattice constant in the range $5.90 < a < 6.025$ a.u., which is a double-moment region.

In addition to the band calculations, Ref. 10 presents calculations of the wave vector dependent enhanced magnetic susceptibility. Based on the magnetic moment and susceptibility

calculations, we predicted the occurrence of ferromagnetism in bcc Mn at low temperature.

For fcc Mn, on the other hand, the moment is found to be zero in the range $6.50 < a < \sim 7.275$ a.u. and large in the region $a > \sim 7.275$ a.u., with a discontinuous zero moment to high moment transition occurring near $a = 7.275$ a.u.

We were able to explain both phase transitions in detail based on the analysis of the band structure. The results presented in this dissertation are being reported in Refs. 46 and 47.

Recently, Marcus and Moruzzi[21] used the fixed moment approach of the ASW method mentioned earlier to determine the total energy of bcc Mn in the paramagnetic and ferromagnetic states as a function of the Wigner-Seitz radius. They determined the ground state to be ferromagnetic, with a small moment ($m \simeq 0.6\ \mu_B$) at a Wigner-Seitz radius of 2.6 a.u. In addition, they found a transition to a high moment phase at an expansion of about 10% in the Wigner-Seitz radius.

The rest of the dissertation is organized as follows. Chapter II presents the theoretical grounds for the calculation, namely, a brief description of the LCGO method and the local density exchange-correlation potential used in the calculation. Chapter III describes the method of calculation, including a brief review of the program used.

The main body of the dissertation is Chapter IV, in which we present the results for the electronic band structure, magnetic moment, and density of states for bcc and fcc manganese as a function of the lattice constant. The different phase transitions occuring

are explained in terms of the details of the calculated band structure. Finally, Chapter V includes a brief discussion of the results and suggestions for future work.

CHAPTER II

THEORY

Nowadays, most of the calculations of the electronic band structure of metals are performed by solving the Kohn-Sham equations[22] of density functional theory.[22,23,24]

The Kohn and Sham equations contain an unknown functional of the density of electrons, namely the exchange-correlation potential. In order to solve those equations and calculate the electronic band structure, a certain form of the exchange-correlation potential must be assumed. Once this is done, the solution can be achieved by several different methods. A review of the different methods of calculation was given by Callaway.[25]

In our calculation, we have used the linear combination of gaussian orbitals (LCGO) method, which is described in the first section of this chapter. The particular form of the exchange-correlation potential chosen is presented in the second section.

A. The LCGO Method.

The single-particle Schroedinger equation to be solved can be written as

$$(-\nabla^2 + V_\sigma(\vec{r}))\ \psi_n(\vec{k},\vec{r}) = E_n(\vec{k})\ \psi_n(\vec{k},\vec{r})\ , \qquad (1)$$

in which $V_\sigma(\vec{r})$ is the spin-dependent effective potential:

$$V_\sigma(\vec{r}) = -\sum_\mu \frac{2Z}{|\vec{r} - \vec{R}_\mu|} + 2\int \frac{\rho(\vec{r})\, d^3r'}{|\vec{r} - \vec{r}'|} + V_{xc,\sigma}(\vec{r}) \ . \quad (2)$$

In these equations, σ is the spin index, n is the band index, Z is the atomic number, and xc stands for exchange-correlation. The vector $\vec{r}$ is the coordinate of a general point, while $\vec{R}_\mu$ is the coordinate of a lattice site, and $\vec{k}$ is the coordinate of a general point in reciprocal space.

The wave-function $\psi_n(\vec{k},\vec{r})$ is a Bloch function, since the potential has the translational symmetry of the lattice. Hence

$$\psi_n(\vec{k}, \vec{r} + \vec{R}_\mu) = e^{i\vec{k}\cdot\vec{R}_\mu} \psi_n(\vec{k},\vec{r}) \ . \quad (3)$$

Atomic units have been used, with energies in Rydbergs (Ry) and distances in atomic units (a.u.). In this system of units $\hbar$=c=1, e^2=2, and m=½.

The LCGO method belongs to a more general family of methods of calculation of the band structure, the so-called tight-binding method.[28] In the tight-binding method, the wave function $\psi_n(\vec{k},\vec{r})$ is first expanded in a finite set of basis functions $\phi_j(\vec{k},\vec{r})$, satisfying the Bloch theorem, and constructed as a linear combination of primitive orbitals centered in the lattice sites. The wave function $\psi_n(\vec{k},\vec{r})$, expanded in terms of the ϕ_j's, is then introduced in equation (1), and the resulting expression is projected onto an arbitrary basis function ϕ_i, yielding a set of algebraic equations for the coefficients of the expansion.

This set of equations can be treated as a matrix eigenvalue

problem and solved for the energy eigenvalues and eigenvectors by standard computational procedures, as explained below.

The basis functions can be constructed in terms of primitive orbitals $u_j(\vec{r})$, centered in the lattice sites:

$$\phi_j(\vec{k},\vec{r}) = N^{-\frac{1}{2}} \sum_{\mu} e^{i\vec{k}\cdot\vec{R}_\mu} u_j(\vec{r} - \vec{R}_\mu) \ .$$

It can be easily verified that the basis functions constructed in this way obey Bloch's theorem. The primitive orbitals $u_j(\vec{r})$ are generally expressed as

$$u_j(\vec{r}) = R_{\ell_j}(r)\ K_{\ell_j,m}\ (\theta,\psi) \ , \qquad (5)$$

in which R_{ℓ_j} and $K_{\ell_j,m}$ are the radial and angular part, respectively. The indices ℓ_j and m correspond to the orbital quantum number and magnetic quantum number, respectively.

The radial functions may be taken to be atomic orbitals, in which case the method of solution is referred to as the linear combination of atomic orbitals (LCAO) method. Or they may be members of a discrete set of functions such as Slater-type orbital ($r^n\ e^{-\alpha r}$) and Gaussian type orbitals ($r^n\ e^{-\alpha r^2}$).

In our calculation, we use gaussian orbitals, which present the advantage that most of the integrals arising in the calculation can be solved analytically. The radial part in the LCGO method is taken to be

$$R_{\ell_j}(r) = N_j\, r^{\ell_j}\, e^{-\alpha_j r^2} \quad , \tag{6}$$

where N_j is a normalization constant.

The angular part $K_{\ell_j,m}(\theta,\psi)$ is often chosen to be a linear combination of spherical harmonics, having the symmetry of the crystal. For the particular case of cubic crystals, the symmetrized angular functions were determined by von der Lage and Bethe[26] and are called Kubic harmonics.

Having described the construction of the basis functions, we can discuss in more detail the method of solution, mentioned above.

The wave function $\psi_n(\vec{k},\vec{r})$ is expanded in term of the basis functions:

$$\Psi_n(\vec{k},\vec{r}) = \sum_j C_{nj}(\vec{k})\, \phi_j(\vec{k},\vec{r}) \quad , \tag{7}$$

in which the $C_{nj}(\vec{k})$ are the coefficients of the expansion.

The substitution of this expression in equation (1), followed by a projection on an arbitrary basis function ϕ_i, yields the matrix equation

$$\sum_j H_{ij}(\vec{k})\, C_{nj}(\vec{k}) = E_n(\vec{k}) \sum_j S_{ij}(\vec{k})\, C_{nj}(\vec{k}) \quad , \tag{8}$$

where $H_{ij}(\vec{k})$ and $S_{ij}(\vec{k})$ are the hamiltonian and unity (overlap) matrices, respectively:

$$H_{ij}(\vec{k}) = \sum_\mu e^{-i\vec{k}\cdot\vec{R}_\mu} \langle u_i(\vec{r}-R_\mu) | -\nabla^2 + V_\sigma(\vec{r}) | u_j(\vec{r}) \rangle \quad , \tag{9}$$

$$S_{ij}(\vec{k}) = \sum_{\mu} e^{-i\vec{k}\cdot\vec{R}_{\mu}} \langle u_i(\vec{r}-\vec{R}_{\mu}) | u_j(\vec{r}) \rangle \ . \qquad (10)$$

The matrix equation (8) can be solved for the eigenvalues $E_n(\vec{k})$ and the eigenvectors, which are given in terms of the coefficients $C_{nj}(\vec{k})$.

The hamiltonian and overlap matrix elements, however, can be calculated only after the potential $V_{\sigma}(\vec{r})$ is known. But this is a functional of the density of electrons.

The problem then, has to be solved self-consistently: a starting potential is constructed generally by superposing atomic wave functions centered on the lattice sites; the overlap and hamiltonian matrices are then calculated, and the eigenvalue problem of equation (8) is solved. The new potential is then constructed and the process is repeated until the new and the old potentials are equal, within the desired precision. The detailed way in which this is done in our calculation is explained elsewhere.[27]

B. The RSK Exchange-Correlation Potential.

As it was stated in the last section, the Kohn-Sham equations include the exchange-correlation potential, which is an unknown functional of the density of states. An approximation, to this functional is then needed to carry on the calculation. Kohn and Sham[22] suggested the local density approximation, which is strictly valid for slowly varying charge density. In this approximation the exchange-correlation functional is written as

$$E_{xc}[\rho] \simeq \int \rho(r)\ \varepsilon_{xc}^{h}\ (\rho(\vec{r}))\ ,$$

where $\varepsilon_{xc}^{h}(\rho)$ is the contribution of exchange and correlation to the total energy per electron in a homogeneous, interacting electron gas of density ρ. The function $\varepsilon_{xc}^{h}(\rho)$ is known only approximately. The local density approximation is the most widely used in band calculations, with several different forms of the function $\varepsilon_{xc}^{h}(\rho)$ being used.

In our calculation we have used the exchange-correlation potential presented by Von Barth and Hedin (VBH),[29] as parametrized by Rajagopal, Singhal, and Kimball (RSK).[30]

This form of the exchange-correlation potential is spin dependent. This produces a splitting of equation (1) into two, one for each spin. In a ferromagnetic calculation, this feature is crucial in generating different energy bands for the majority and minority spin, the so-called exchange splitting.

According to Von Barth and Hedin,[29] the exchange-correlation potential can be written as

$$V_{xc,\sigma}(\vec{r}) = \frac{\partial}{\partial \rho_{\sigma}(\vec{r})}\ [\rho(\vec{r})\ e_{xc}(\rho_{+}(\vec{r}),\ \rho_{-}(\vec{r}))]\ ,$$

in which $\rho(\vec{r})$ is the total electron density, equal to the sum of the majority and minority spin densities:

$$\rho(\vec{r}) = \rho_{+}(\vec{r}) + \rho_{-}(\vec{r})$$

and e_{xc} is a functional of the electron density, including contributions from exchange and correlation:

$$e_{xc}(\rho_+(\vec{r}),\ \rho_-(\vec{r})) = e_x + e_c \ .$$

The exchange term can be written as:

$$e_x = -\ 3\ (\frac{3}{4\pi})^{1/3} \cdot (\frac{\rho_+(\vec{r})^{4/3} + \rho_-(\vec{r})^{4/3}}{\rho(\vec{r})}) \ .$$

The correlation term is given by

$$e_c = \varepsilon_c^p + (\varepsilon_c^p - \varepsilon_c^f)\ f(x) \ ,$$

in which the function f is:

$$f(x) = \frac{1}{1-2^{-1/3}}\ (X_+^{4/3} + X_-^{4/3} - 2^{-1/3}) \ ,$$

with the X_+ and X_- being the relative majority and minority spin densities

$$X_+ = \frac{\rho_+(\vec{r})}{\rho(\vec{r})} \text{ and } X_- = \frac{\rho_-(\vec{r})}{\rho(\vec{r})} \ .$$

The quantities ε_c^p and ε_c^f can be expressed in terms of four constants, c^p, r^p, c^f, and r^f, which are the only parameters of the theory. In the VBH potential the values are

$c^p = 0.0504$, $r^p = 30$, $c^f = 0.0254$, $r^f = 75$,

while in the RSK, they are

$c^p = 0.04612$, $r^p = 39.7$, $c^f = 0.02628$, $r^f = 70.6$. More details on local density approximation to the exchange-correlation potential can be found in the reviews by Rajagopal,[30] Callaway and March,[31] and Williams and von Barth.[32]

CHAPTER III

METHOD OF CALCULATION

In this chapter we give a brief description of the numerical techniques used in the solution of the single-particle equations, which were presented in Chapter 2.

The solution is achieved by the use of a package of programs, BNDPKG, developed by Wang and Callaway[27]. This package calculates the energy bands, eigenvectors, and density of states for materials with cubic symmetry and one atom per unit cell. The calculation is nonrelativistic and at zero temperature. Paramagnetic and ferromagnetic orders only are allowed. Antiferromagnetism is not included in the formulation, so a spin-polarized calculation with BNDPKG, predicting a nonzero magnetic moment per atom, cannot rule out the possibility of an antiferromagnetic order.

As was stated on the previous chapter, the eigenvalue problem has to be solved self-consistently. First, a starting charge density is constructed by superposition of gaussian orbitals from atomic calculations. From this, the starting potential is generated, which is then used in the calculation of the overlap and hamiltonian matrices. The problem is then solved by standard diagonalization procedures, and the new charge density and potential are constructed. The process is repeated until convergence.

BNDPKG is divided into several programs corresponding to the

different stages of the calculation.

The first program, FCOF, performs two main tasks. First, it generates a starting charge density by superposing gaussian orbitals from an atomic calculation. The set of the occupation numbers (i.e., the number of electrons to be assigned to every atomic level) is an input of this program. This feature is used in a spin-polarized calculation to set an input magnetic moment by having a larger number of 'spin-up' (majority) electrons than 'spin-down' (minority) electrons. Fractional occupation numbers are permitted, allowing for an input magnetic moment equal to a fractional number of Bohr magnetons.

Once the starting charge density has been constructed, FCOF calculates the Fourier coefficients of the different terms in the potential, namely, the electronic and nuclear Coulomb potential and the exchange-correlation potential. This is done to facilitate the evaluation of the hamiltonian and overlap matrix elements, which, despite their apparent simplicity, contain three-dimensional multi-centered integrals, very hard to evaluate.

This was pointed out by Lafon and Lin,[33] who demonstrated that the expansion of the potential in a Fourier series,

$$V_\sigma(\vec{r}) = \sum_{K_s} V_\sigma(\vec{K}_s) \cos \vec{K}_s \cdot \vec{r} \ ,$$

reduces the complexities of the evaluation of the hamiltonian and overlap matrices to, at most, two-centered integrals. With the use

of gaussian orbitals, all the two-centered integrals can be evaluated analytically.[34,35,36] Only cosine terms need to be considered in the Fourier expansion of the potential. This is justified because the potential has inversion symmetry.

The program ESINT evaluates the overlap and hamiltonian integrals needed in the calculation of the corresponding matrix elements.

The third program, BND, generates the overlap and hamiltonian matrix elements by summing over lattice sites, the integrals calculated in ESINT, with the appropriate Bloch phase factor. The use of the rotational symmetry properties of the hamiltonian and of the orbitals greatly simplifies the calculation. Program BND also provides an option to diagonalize the hamiltonian at this point, if only evaluation of the bands is needed. This feature is used after self-consistency is achieved, to generate the final bands in a larger number of points of the irreducible wedge of the Brillouin zone.

The next two programs, SIJ and INVSIJ, generate the so-called generalized overlap matrices which are used in the iterations toward self-consistency to calculate the changes in the Fourier coefficients.

The iterative process is performed by two programs, SCF1 and SFC2, for the paramagnetic and ferromagnetic calculation, respectively. The changes on the Fourier coefficients of the charge density, and those of the Coulomb and exchange-correlation

potentials, are calculated at every iteration. These quantities are then added to the corresponding values coming from the last iteration to construct the new hamiltonian and overlap matrices. A damping factor can be introduced to reduce oscillations in the iterative process and to accelerate the convergence. A damping factor between 0.2 and 0.3 has been used with good results.

Since we were interested in the calculation of the magnetic moment, our criterion for convergence was a variation of less than 10^{-4} μ_B in the magnetic moment. This is, in general, a much more stringent criterion than the one used in past calculations, namely variations of less than 10^{-4} in the Fourier coefficients. The number of iterations required in our calculations ranged from 100 to 250.

After self-consistency is achieved, the program ESINT is used again to generate the final version of the energy and overlap integrals, which are then introduced in the program BND to construct the final matrix elements. The hamiltonian is then diagonalized at the selected points of the irreducible wedge of the Brillouin zone, to yield the final band structure. The program DENST can then be used to calculate the density of states. Two plotting programs are provided to generate plots of the band structure and density of states.

Our calculations were performed on an IBM 3084 computer. The basis set used consisted of 75 gaussian orbitals. Under these conditions, it took about 50 minutes of CPU time to run the first five programs. In the iterative process, every iteration took an

average of 15 minutes. The final bands were determined at 505 points of the irreducible wedge, for the bcc case, and at 506 points for the fcc structure.

CHAPTER IV

ELECTRONIC AND MAGNETIC STRUCTURE OF BCC AND FCC MANGANESE

In this chapter, we present the results of our calculations of the electronic band structure, magnetic moment, and density of states of bcc and fcc manganese, as a function of the lattice constant.

As explained in the previous chapters, we used the linear combination of gaussian orbitals (LCGO) version of the tight-binding method. The theoretical foundation for the tight-binding method is density functional theory, which states that the properties of the ground state of an inhomogeneous electron gas are a unique functional of the density of electrons. This applies in particular to the exchange-correlation potential, although the true functional is unknown. Different approximations for the exchange-correlation potential have been presented, most of which belong to the local-density type. In our calculation, we have used the exchange-correlation potential of von Barth and Hedin[29] in the parametrization of Rajagopal, Singhal and Kimball.[30]

The calculations were performed using the program BNDPKG by Wang and Callaway,[27] as explained in Chapter III. The basis set consisted of gaussian type orbitals for the manganese atom, as calculated by Watchers.[37] However, we dropped the most diffuse s-orbital, and we added one p-orbital. One single f-orbital was also incorporated, yielding a basis set composed of 13s, 10p, 5d, and 1f-orbitals, which make a total of 75 (uncontracted) basis functions.

The input electronic configuration was taken to be $3d^6$, $4s^1$, for both bcc and fcc Mn. An input value for the magnetic moment must be set in BNDPKG by fixing different occupation numbers for the majority- and minority-spin 3d levels. In most of the calculations, the input moment was taken to be $2.4\mu_B$ (corresponding to occupation numbers of 4.2 and 1.8 for the majority- and minority-spin 3d levels, respectively). The choice of the input magnetic moment has, in general, no important effect, other than to accelerate the convergence of the iterative process when a good guess is made. However, a special situation may occur when two local minima of the total energy coexist at the same atomic volume, having different values of the magnetic moment. A situation like this has been reported by Moruzzi and coworkers in their calculation of the total energy of fcc Fe.[38] They found a double-moment region to occur in a small range of lattice constants, in which two magnetic phases, a 'high-spin' and a 'low-spin' state coexist.

In our calculations for bcc manganese, we found a small range of lattice constants in which the magnetic moment converged to two different values, according to the choice of the input moment. We were not able, however, to decide which one of the two values corresponds to a lower energy state, since we did not calculate the total energy. We determined that the double-moment region extends from $a = 5.900$ to 6.025 a.u. ($r_s \simeq 2.90$ to 2.97 a.u.). At some lattice constant within this range, there is an abrupt transition from the low moment to the high moment state.

During the iterations, the bands were calculated in 55 points of

the irreducible wedge of the Brillouin zone for bcc Mn and in 89 points for fcc Mn. The final bands were generated in 506 and 505 points, respectively, for bcc and fcc manganese.

The convergence criterion was a variation of less than $10^{-4}\mu_B$ in the magnetic moment.

A range of lattice constants from 5.2 to 8.0 a.u. (r_s = 2.56 to 3.94 a.u.) was considered for bcc Mn. For fcc Mn the range was from 6.5 to 9.0 a.u. ($r_s \simeq$ 2.54 to 3.52 a.u.)

The main purpose of our calculations was to investigate the existence of different magnetic phases in bcc and fcc manganese when the lattice constant is varied through the ranges indicated in the previous paragraph. In the case of bcc manganese, we found that there is a transition from a low moment to a high moment state at some lattice constant in the range a = 5.9 to 6.025 a.u. ($r_s \simeq$ 2.90 to 2.97 a.u.). On the other hand, for fcc manganese there is a transition from a zero moment to a high moment region at a lattice constant of about 7.25 a.u. ($r_s \simeq$ 2.83 a.u.). Since our calculation does not allow for antiferromagnetic order, it cannot distinguish between ferro- and antiferromagnetism. However, the susceptibility calculation done by Fry and coworkers[10] for a lattice constant of 5.397 a.u. (r_s = 2.66 a.u.) seems to indicate that bcc manganese is ferromagnetic in the low moment region.

Section A contains the results of our calculations for bcc manganese, while section B gives those for fcc manganese.

A. BCC Manganese

The electronic band structure, magnetic moment, and density of states of bcc manganese were determined for a number of lattice constants ranging from 5.2 a.u. (the calculated paramagnetic equilibrium value)[39] to 8.0 a.u. ($r_s \simeq 2.56$ to 3.94 a.u.). Some representative values of the exchange splitting and band width are given for several lattice constants in Tables I and II.

Table III gives the magnetic moment of bcc Mn as a function of the lattice constant. As explained in the introduction to this chapter, we found that bcc manganese can exist in two different magnetic phases, namely a low moment and a high moment state. The magnetic moment for every one of these phases is presented in separate columns, since there is a small range of lattice constants, from a = 5.900 to 6.025 a.u. ($r_s \simeq 2.90$ to 2.97 a.u.), in which the two phases can coexist. Within this range, the magnetic moment converged, either to a low or to a high value, according to the input moment chosen. Outside this 'double-moment region,' the magnetic moment always converged to the same value, even when the calculation was repeated using a substantially different input moment.

Figure 1 shows the magnetic moment versus lattice constant for bcc manganese. Figure 1 stresses the fact that the magnetic moment is nonzero for the whole range of lattice constants considered, and that there are two magnetic phases, one with a low moment and the other with a high moment. The 'double-moment region,' between a = 5.9 and 6.025 a.u., corresponds to the coexistence of two local minima of the total energy for the same values of the lattice

a (a.u.)	r_s (a.u.)	δE_{ex} (Ry)					
		Γ_1	N_1	P_4	P_3	H_{12}	H_{25}'
5.2	2.560	-0.0032	0.0255	0.0301	0.0653	0.0357	0.0554
5.8	2.856	-0.0005	0.0427	0.0484	0.0977	0.0673	0.0808
5.925	2.917	0.0001	0.0461	0.0520	0.1039	0.0750	0.0854
5.95	2.930	0.0480	0.1242	0.1401	0.2077	0.1598	0.2053
6.0	2.954	0.0570	0.1381	0.1562	0.2232	0.1749	0.2276
8.0	3.939	0.0693	0.2084	0.2493	0.3025	0.3000	0.2997

Table I. Representative exchange splittings (δE_{ex}) for bcc manganese, at various lattice constants (a). The Wigner-Seitz radii (r_s) are also given.

a (a.u.)	r_s (a.u.)	W(Ry)					
		$(H_{15\downarrow} - \Gamma_{1\downarrow})$	$(P_{3\uparrow} - P_{4\uparrow})$	$(P_{3\downarrow} - P_{4\downarrow})$	$(P_{3\downarrow} - P_{4\uparrow})$	$(H_{25'\uparrow} - H_{12\uparrow})$	$(H_{25'\downarrow} - H_{12\downarrow})$
5.2	2.560	1.4327	0.2627	0.2979	0.3280	0.4881	0.5078
5.8	2.856	1.1425	0.1646	0.2138	0.2622	0.2872	0.3007
5.925	2.917	1.0927	0.1491	0.2010	0.2530	0.2553	0.2655
5.95	2.930	1.0906	0.1544	0.2220	0.3620	0.2471	0.2607
6.0	2.954	1.0731	0.1527	0.2197	0.3760	0.2338	0.2864
8.0	3.939	0.5970	0.0226	0.0758	0.3251	0.0189	0.0186

Table II. Representative band widths (W) for bcc manganese, at various lattice constants (a). The Wigner-Seitz radii (r_s) are also given. Spin up and down are indicated by $\uparrow$ and $\downarrow$, respectively.

a (a.u.)	m_1 (μ_B)	m_2 (μ_B)
5.200	0.76	
5.397	0.93	
5.450	0.97	
5.628	1.09	
5.800	1.18	
5.900	1.24	2.40
5.925	1.26	2.93
5.950	1.28	3.12
5.975	1.29	3.40
6.000	1.32	3.49
6.025	1.35	3.53
6.050		3.56
7.000		4.37
8.000		4.93

Table III. Lattice constant a and magnetic moment m for bcc Mn. Indices 1 and 2 refer to the low moment and high moment states, respectively.

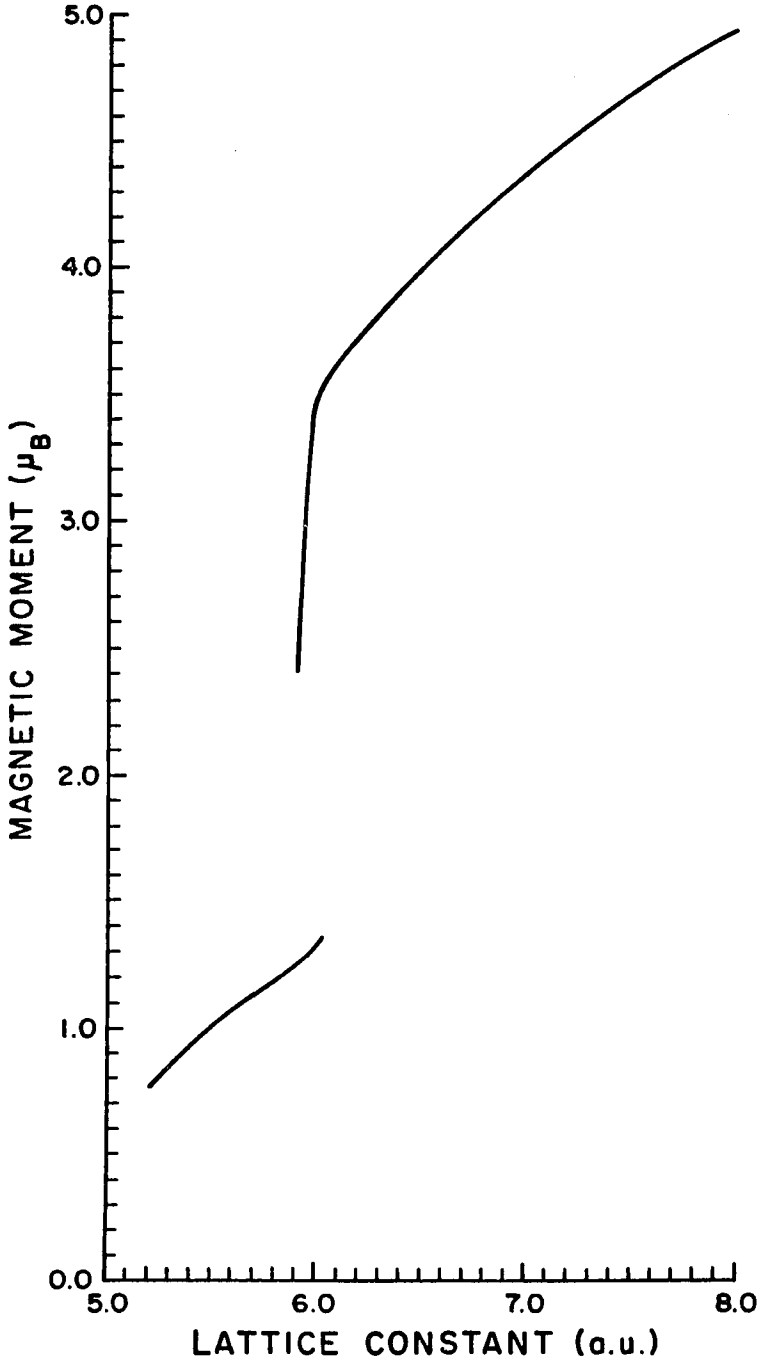

Figure 1. Magnetic moment as a function of lattice constant for bcc Mn.

constant. Somewhere in that region, there must be a transition from the low moment to the high moment phase, at a certain lattice constant which we could not determine since we did not perform a calculation of the total energy. As our program only allows paramagnetic and ferromagnetic ordering, we were not able to identify these two phases as being either ferro- or antiferromagnetic. Fry and coworkers[10] presented a calculation of the random-phase-approximation susceptibility (χ_0) and many-body-enhanced susceptibility (χ) versus the wavevector $\vec{q}$ along one of the cubic axes, for a lattice constant of 5.397 (a.u.) ($r_s \simeq 2.66$ a.u.) in the region of low magnetic moment. The fact that χ_0 is monotonically decreasing, together with χ having a singularity and being negative at q=0, indicates that the low moment state should be ferromagnetic. This agrees with the results of Kübler[8] and Marcus and Moruzzi[21].

The abrupt increase in the magnetic moment can be associated with the changes that occur in the electronic band structure with respect to variations in the atomic volume. In order to describe those changes in detail we have plotted the d-bands for three values of the lattice constant in the range in which the transition occurs. As pointed out before, we did not determine the point at which the transition takes place. Nevertheless, the three points chosen should serve well to illustrate how the transition occurs.

Figure 2 gives the majority-spin bands for bcc Mn at the lattice constants of 5.925 a.u. (in the low moment state), 5.95 a.u. (in the high moment state) and 6.0 a.u. (in the high moment state), corresponding to Wigner-Seitz radius of $r_s \simeq 2.92$, 2.93, and 2.95

a.u., respectively. Figure 3 gives the minority-spin bands for the same values of the lattice constant. The density of states for bcc Mn, at those three values of the lattice constant, is shown in Figure 4 for both spins.

The abrupt increase in the magnetic moment can be related to large, almost flat regions of the majority-spin bands being filled, while similar regions of the minority-spin bands are being depleted, as the lattice constant increases. The major features of the band structure can be identified in the bands and density-of-states curves corresponding to a = 5.925 a.u. (upper part of Figs. 2, 3, and 4, respectively). In the first place, there is a very sharp and high peak in the majority-spin density of states centered at an energy of about -0.23 Ry, just above the Fermi level. This peak is associated with the almost flat portion of the D_2 band, between the points N_4 and P_3 of the majority-spin bands (top of Fig. 2). A second feature of the majority bands that plays a role in the transition is the 'shoulder' located approximately between energies of -0.21 and -0.16 Ry, which is mainly related to the states around the point H_{25}'. The minority-spin density-of-states curve, on the other hand, presents a deep 'valley' at the Fermi level and a complex structure located approximately between E = -0.25 and -0.33 Ry, containing two main peaks at about -0.37 and -0.31 Ry, respectively. This complex structure is made up of contributions from the states around Γ_{25}' on one side, and from the states around N_2 and P_4 on the other (top of Fig. 3).

The transition from a low moment to a high moment state can then

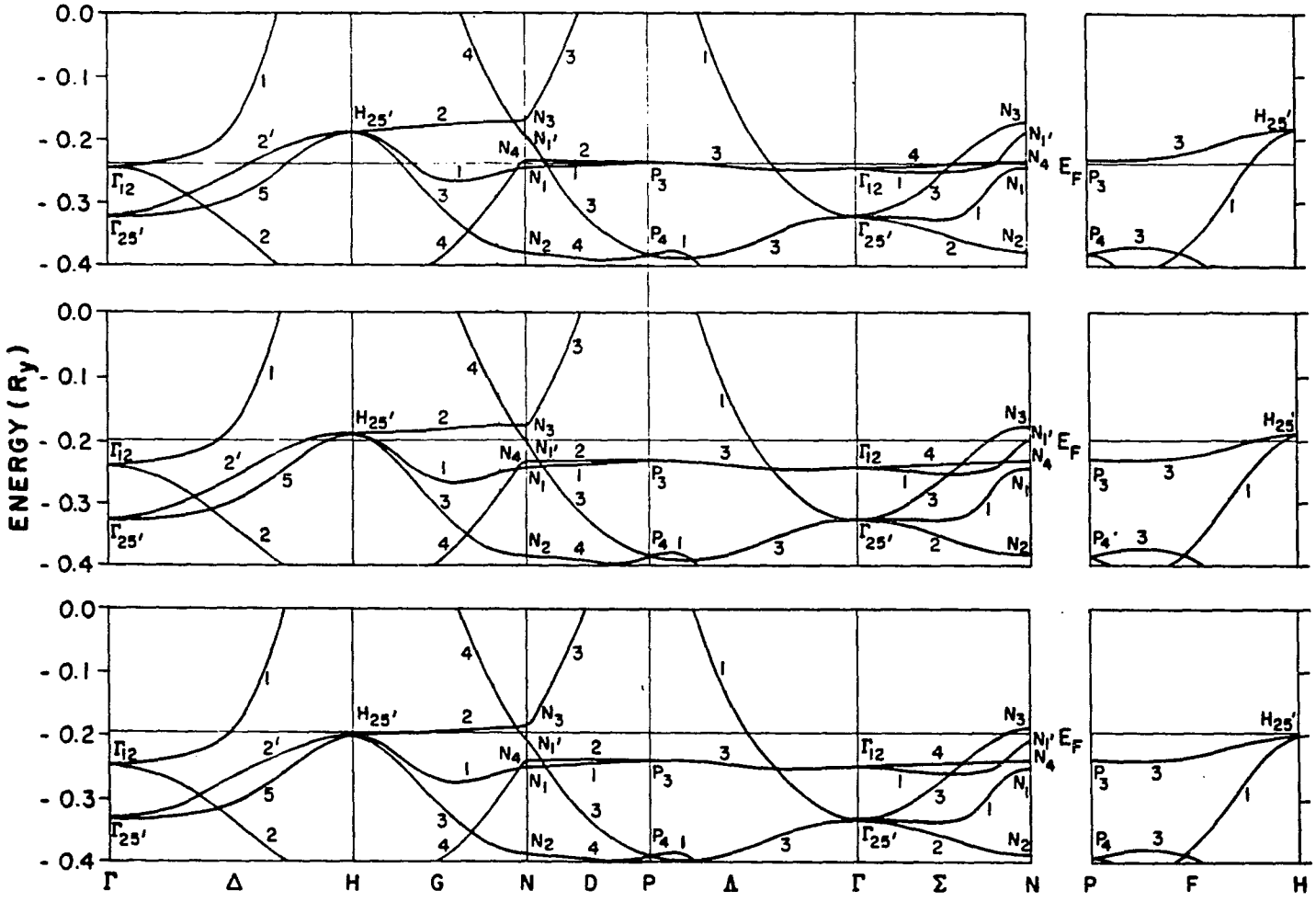

Figure 2. Majority-spin band structure of bcc Mn at lattice constants of 5.925 a.u. (top), 5.950 a.u. (middle), and 6.000 a.u. (bottom).

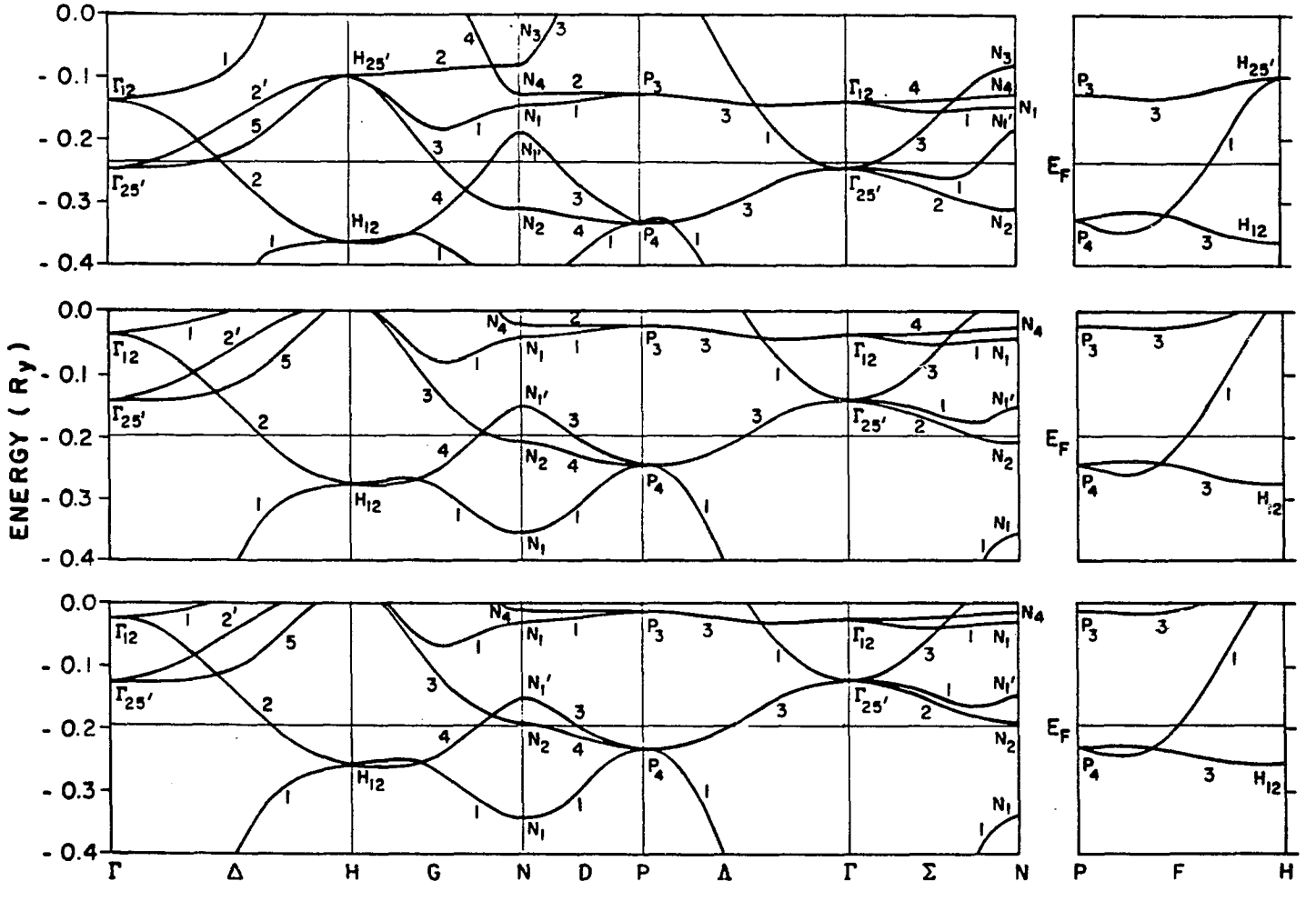

Figure 3. Minority-spin band structure of bcc Mn at lattice constants of 5.925 a.u. (top), 5.950 (middle), and 6.000 a.u. (bottom).

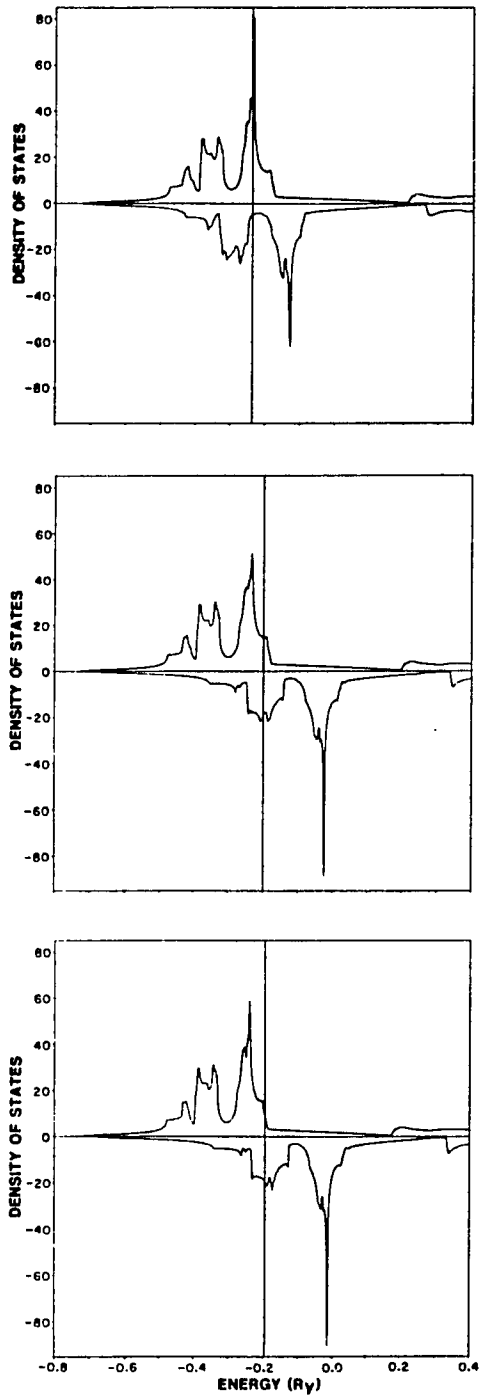

Figure 4. Density of states of bcc Mn (both spins) at lattice constants of 5.925 a.u. (top), 5.950 a.u. (middle), and 6,000 a.u. (bottom).

be described as follows. In a first stage, as the lattice constant increases from 5.925 to 5.95 a.u. (top and middle part of Figs. 2, 3 and 4), the sharp peak of the majority-spin density of states totally fills up, together with a small protion of the 'shoulder.' This is done at the expense of the minority-spin states, which are emptied, as more than half of the complex structure is shifted over the Fermi level. The transformations just described are responsible for the jump in the magnetic moment from 1.26 to $3.12\mu_B$. In a further development, as the lattice constant continues to expand from a = 5.95 to 6.0 a.u., almost all the states contained in the shoulder become filled, while more states in the complex structure are depleted accordingly. A further increase in the lattice constant beyond 6.0 a.u. should bring the rest of the majority-spin shoulder under the Fermi level, while the rest of the minority complex structure is depleted, causing a further, gradual increase in the magnetic moment, which gets closer to the maximum possible value for an isolated atom, namely $5\mu_B$.

Figures 5 and 6 show the majority- and minority-spin bands for a lattice constant of 8.0 a.u., at which the moment is $4.93\mu_B$. It can be seen that the d-bands have become almost completely flat and concentrated in a narrow range of energies. The majority-spin d-bands are now completely filled, while the minority d-bands are almost completely empty, in a highly localized, atom-like picture.

We have described in detail the transformations of the band structure which explain the sharp transition from a low moment to a high moment state of bcc manganese.

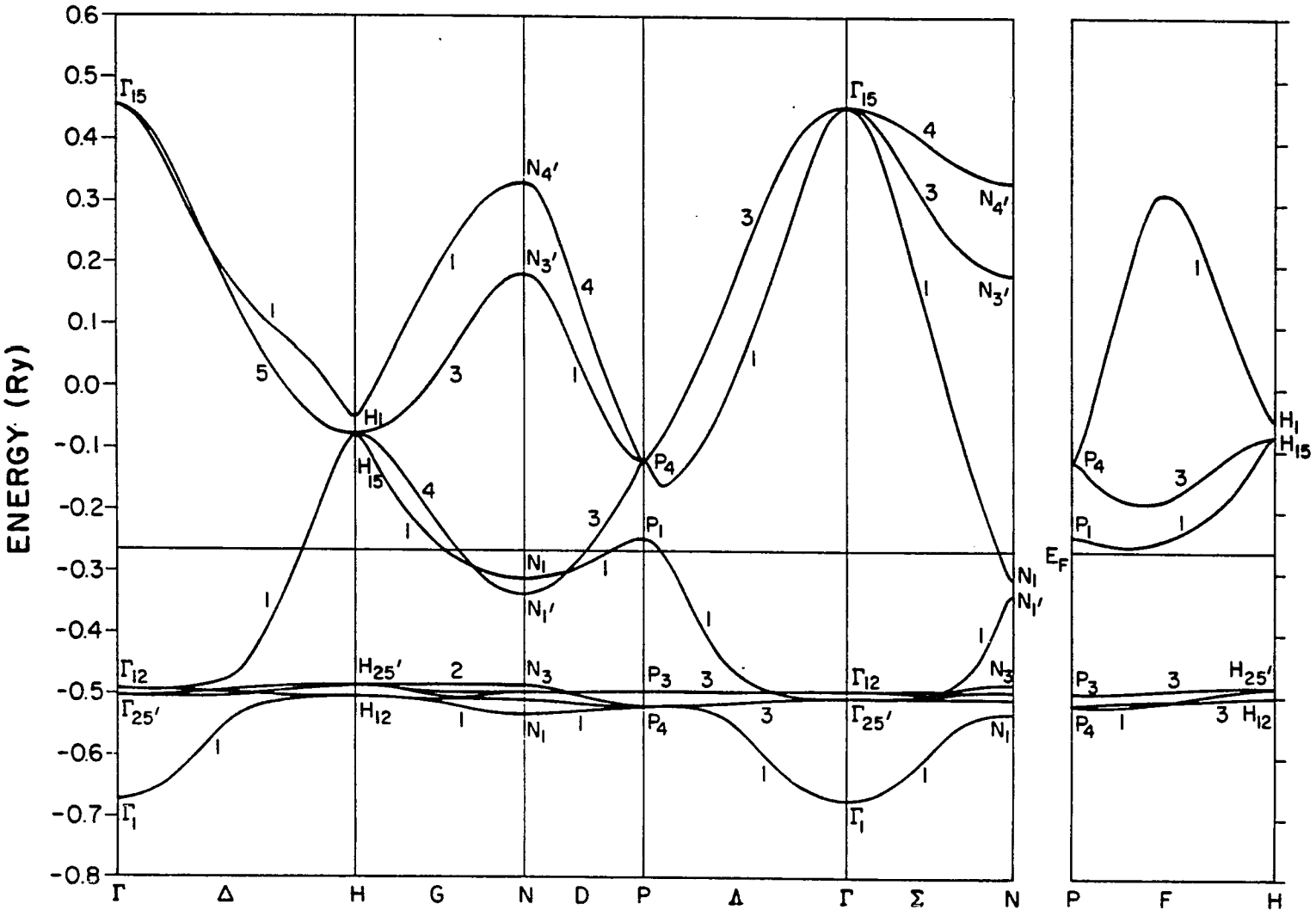

Figure 5. Majority-spin band structure of bcc Mn at the lattice constant of 8.0 a.u.

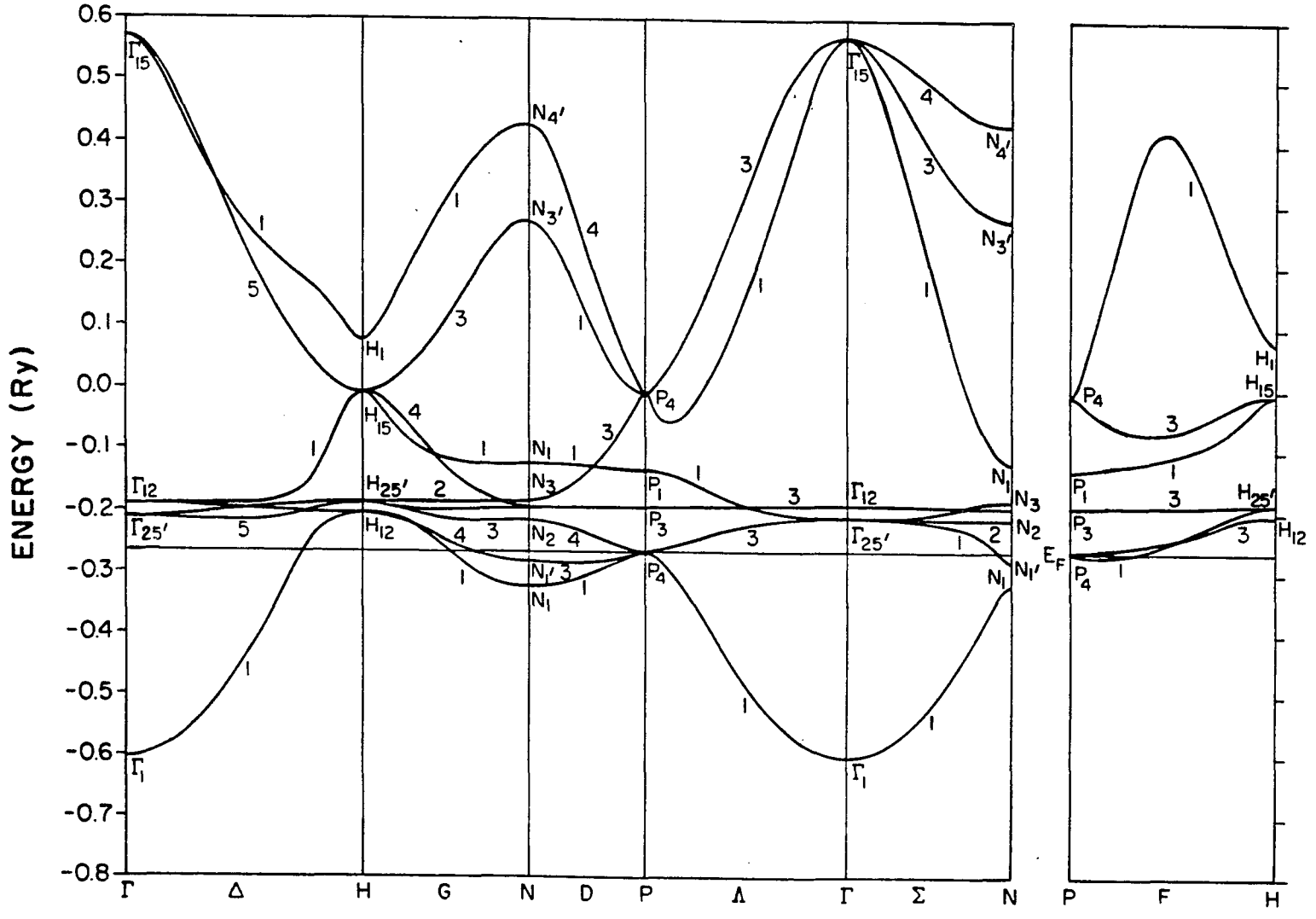

Figure 6. Minority-spin band structure of bcc Mn at the lattice constant of 8.0 a.u.

Since our band calculation does not include antiferromagnetism, it cannot identify the magnetic phases as being either ferromagnetic or antiferromagnetic. The susceptibility calculation, however, indicates that the low moment state of bcc Mn is ferromagnetic. A generalization of BNDPKG to include antiferromagneism would be highly desirable. This, followed by a calculation of the total energy for all three magnetic phases, would give us a much more complete picture of the magnetic structure of bcc manganese.

As mentioned in Chapter I, bcc manganese has been synthesized by epitaxial growing on a (001) iron substrate.[6] If we assume that the lattice constant of the Mn layers is about the same as that of the substrate, then bcc Mn with a lattice constant of approximately 5.4 a.u. has been produced. No magnetic moment was observed, however. The meaning of this result is inconclusive and more experimental work is needed, especially in growing bcc Mn on a variety of substrates with different interatomic spacing. This may not be a simple task, though, as the bcc structure may become more difficult to stabilize at larger lattice constants.

The former discussion should lead us to conclude that the field is open to both theoretical and experimental developments.

B. FCC Manganese

The spin polarized band structure, magnetic moment, and density of states of fcc manganese were determined for several lattice constants ranging from 6.5 to 9.0 a.u. ($r_s \approx 2.54$ to 3.52 a.u.).

Some representatives values of the exchange splitting and band width for several lattice constants are given in Tables IV and V.

Table VI gives the magnetic moment for fcc Mn as a function of lattice constant. Also given in Table VI is the bcc equal volume lattice constant a_{bcc}, which is defined as the fcc lattice constant divided by $2^{1/3}$.

The magnetic moment is plotted in Fig. 7 as a function of the lattice constant. The magnetic moment is zero for the region between a = 6.5 a.u. and 7.25 a.u. (r_s = 2.54 and 2.83 a.u.), with an abrupt increase to a high value, comparable to that of bcc manganese in the high moment state.

It is interesting to compare the magnetic moment curves for the bcc and fcc cases, in the high moment region. Figure 8 shows the magnetic moment as a function of lattice constant for bcc (solid line) and fcc (dashed line) Mn, where the fcc curve is plotted versus the bcc equal volume lattice constant to facilitate the comparison of the two curves.

The striking similarity of the magnetic moment curves for bcc and fcc Mn in the high moment region suggests that the sharp increase in the moment is an effect related to the change in the atomic volume and not to the particular details of the crystal structure.

a (a.u.)	r_s (a.u.)	δ_{ex}(Ry)					
		$\Gamma_{25'}$	Γ_{12}	X_3	X_2	L_3 (lowest)	L_3 (highest)
7.0	2.736	0.0001	0.0002	0.0001	0.0003	0.0002	0.0002
7.2	2.814	0.002	0.0004	0.0002	0.0004	0.0003	0.0003
7.3	2.853	0.1038	0.1442	0.0877	0.1507	0.1201	0.1309
7.5	2.931	0.1982	0.2229	0.1741	0.1980	0.2029	0.2246

Table IV. Representative exchange splittings (δE_{ex}) for fcc manganese at various lattice constants (a). The Wigner-Seitz radii (r_s) are also given.

a (a.u.)	r_s (a.u.)	W (Ry)					
		$(X_{4'\downarrow} - \Gamma_{1\downarrow})$	$(X_{2\uparrow} - X_{3\uparrow})$	$(X_{2\downarrow} - X_{3\downarrow})$	$(X_{2\downarrow} - X_{3\uparrow})$	$(X_{5\uparrow} - X_{1\uparrow})$	$(X_{5\downarrow} - X_{1\downarrow})$
7.0	2.736	0.7619	0.3248	0.3250	0.3251	0.3890	0.3891
7.2	2.814	0.7155	0.2861	0.2864	0.2865	0.3423	0.3423
7.3	2.853	0.7118	0.2433	0.3063	0.3940	0.3186	0.3422
7.5	2.931	0.7098	0.2445	0.2819	0.4560	0.2783	0.3338

Table V. Representative band widths (W) for fcc manganese at various lattice constants (a). The Wigner-Seitz radii (r_s) are also given. Spin up and down are indicated by $\uparrow$ and $\downarrow$, respectively.

a (a.u.)	a_{bcc} (a.u.)	m (μ_B)
6.50	5.159	0.00
6.75	5.357	0.00
7.000	5.556	0.00
7.200	5.715	0.00
7.250	5.754	0.00
7.275	5.774	1.71
7.300	5.794	1.88
7.400	5.873	2.82
7.450	5.913	3.20
7.500	5.953	3.42
7.600	6.032	3.55
7.700	6.111	3.63
8.000	6.350	3.84
9.000	7.143	4.44

Table VI. Lattice constant a, bcc equal volume lattice constant a_{bcc}, and magnetic moment m for fcc Mn. The bcc equal volume lattice constant is obtained by dividing the fcc lattice constant by $2^{1/3}$.

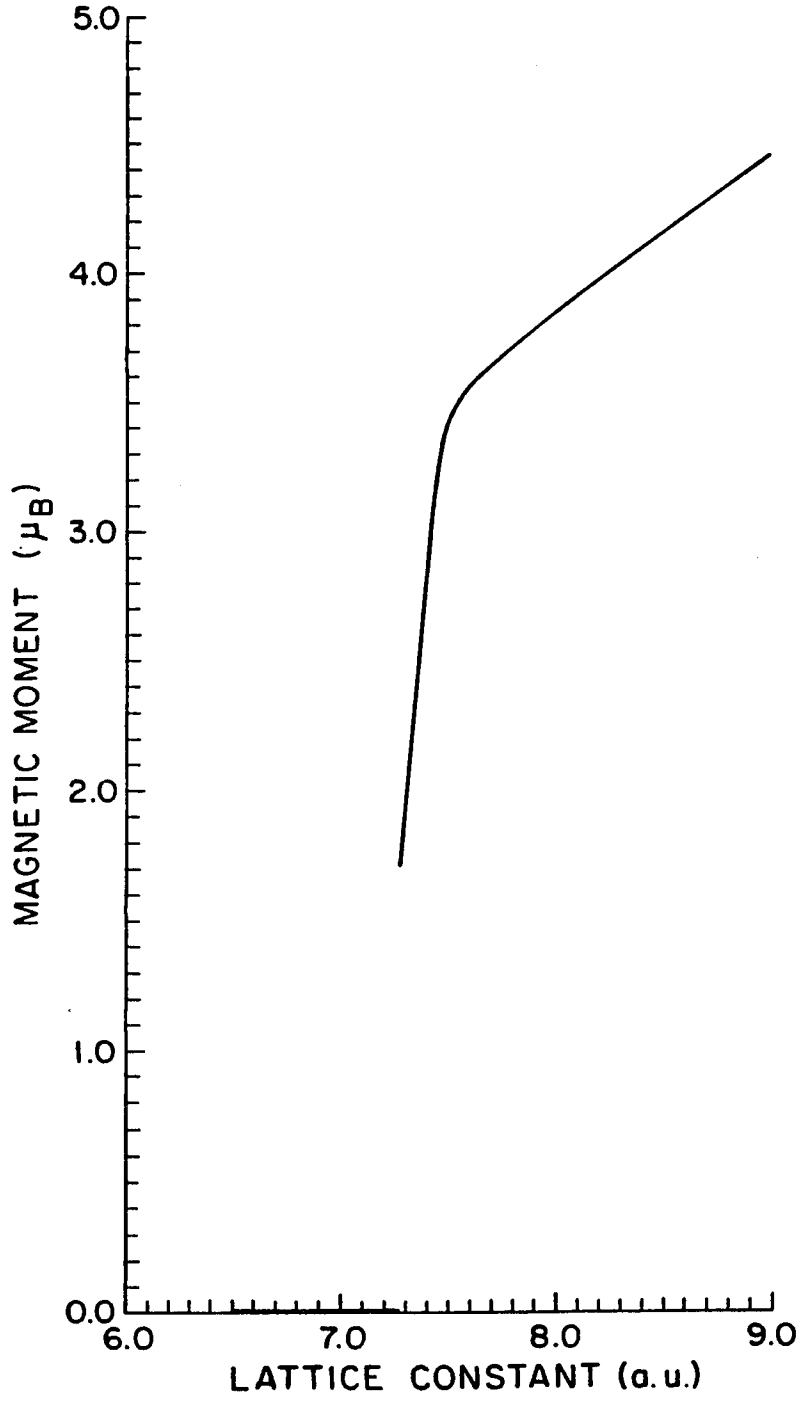

Figure 7. Magnetic moment as a function of lattice constant for fcc Mn.

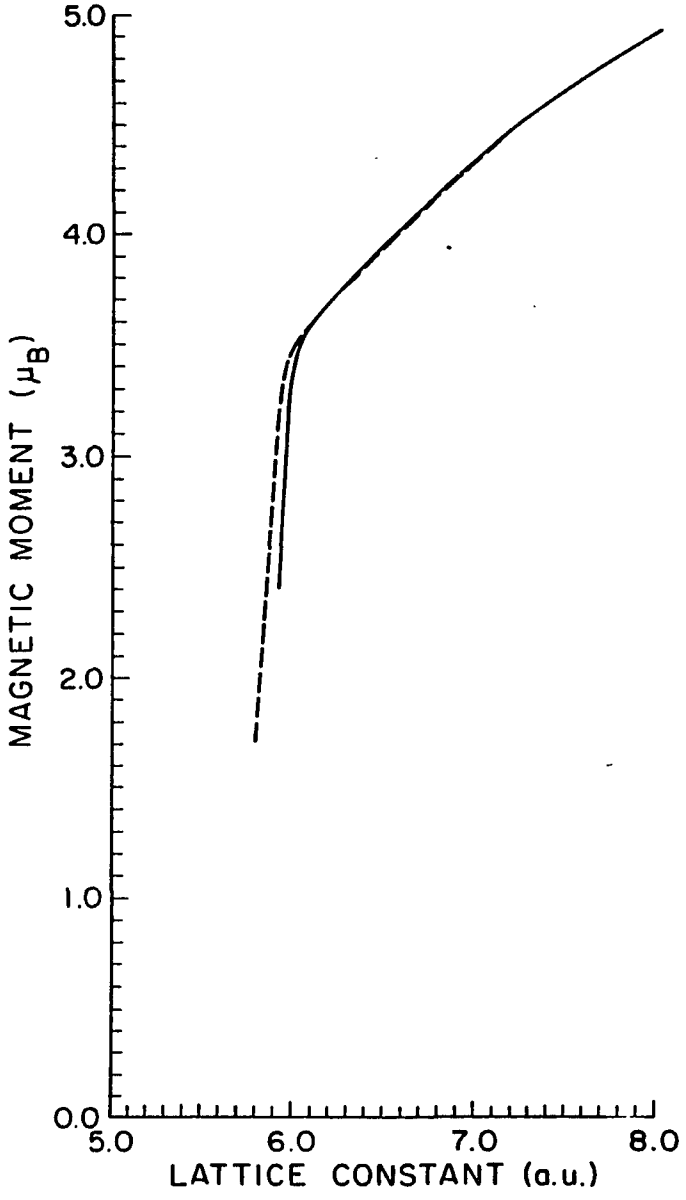

Figure 8. Magnetic moment as a function of lattice constant for bcc (solid line) and fcc (dashed line), in the high moment region. The fcc curve is plotted against the bcc equal volume lattice constant which is obtained dividing the fcc lattice constant by $2^{1/3}$.

Following a similar analysis, as in the case of bcc Mn, we can describe in detail the changes in the band structure that are responsible for the abrupt increase in the magnetic moment. Thus, the spin-polarized energy bands have plotted for three values of the lattice constant in the transition region. Figures 9 and 10 show the majority and minority spin bands, respectively, for lattice constants of 7.2 a.u. (in the zero moment region), 7.3 a.u. (within the transition region, with a moment of $1.88\mu_B$), and 7.5 a.u. (where the magnetic moment is $3.42\mu_B$), ($r_s \simeq 2.81$, 2.85, and 2.93 a.u.). The density-of-states curves for both spins are given in Fig. 11.

By a similar argument, as in the case of bcc Mn, we can describe the sudden jump in the magnetic moment by the existence of large, almost flat regions of the majority-spin bands being filled, while similar regions of the minority-spins bands are being emptied.

The main features of the band structure of fcc Mn that are related to the transition can be discerned on the band and density-of-states curves for the lattice constant 7.2 a.u. (upper part of Figs. 9, 10, and 11).

First, there is a high peak in the majority-spin density of states, centered at about -0.11 Ry. This peak is composed of the states located in the flat region around the point X_2, especially the right portion of the Δ_2 majority band. A more complex structure including two smaller peaks in the majority-spin density is located just above the Fermi energy, approximately between -0.19 and -0.25 Ry. This structure is made up of contributions from the flat portion of the Q_1 band, adjacent to the point W_1, and from regions located

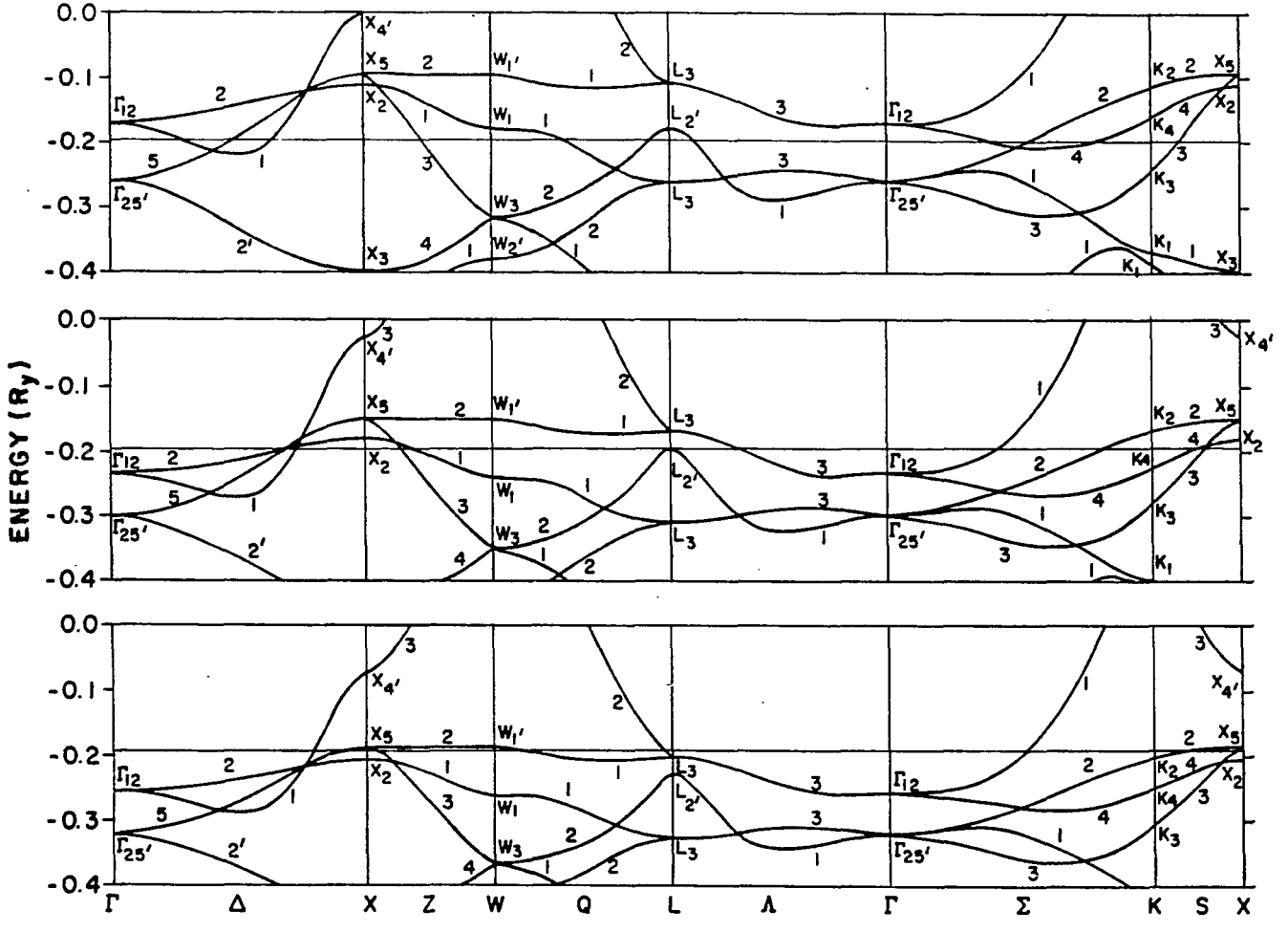

Figure 9. Majority-spin band structure of fcc Mn at lattice constants of 7.2 a.u. (top), 7.3 a.u. (middle), and 7.5 a.u. (bottom).

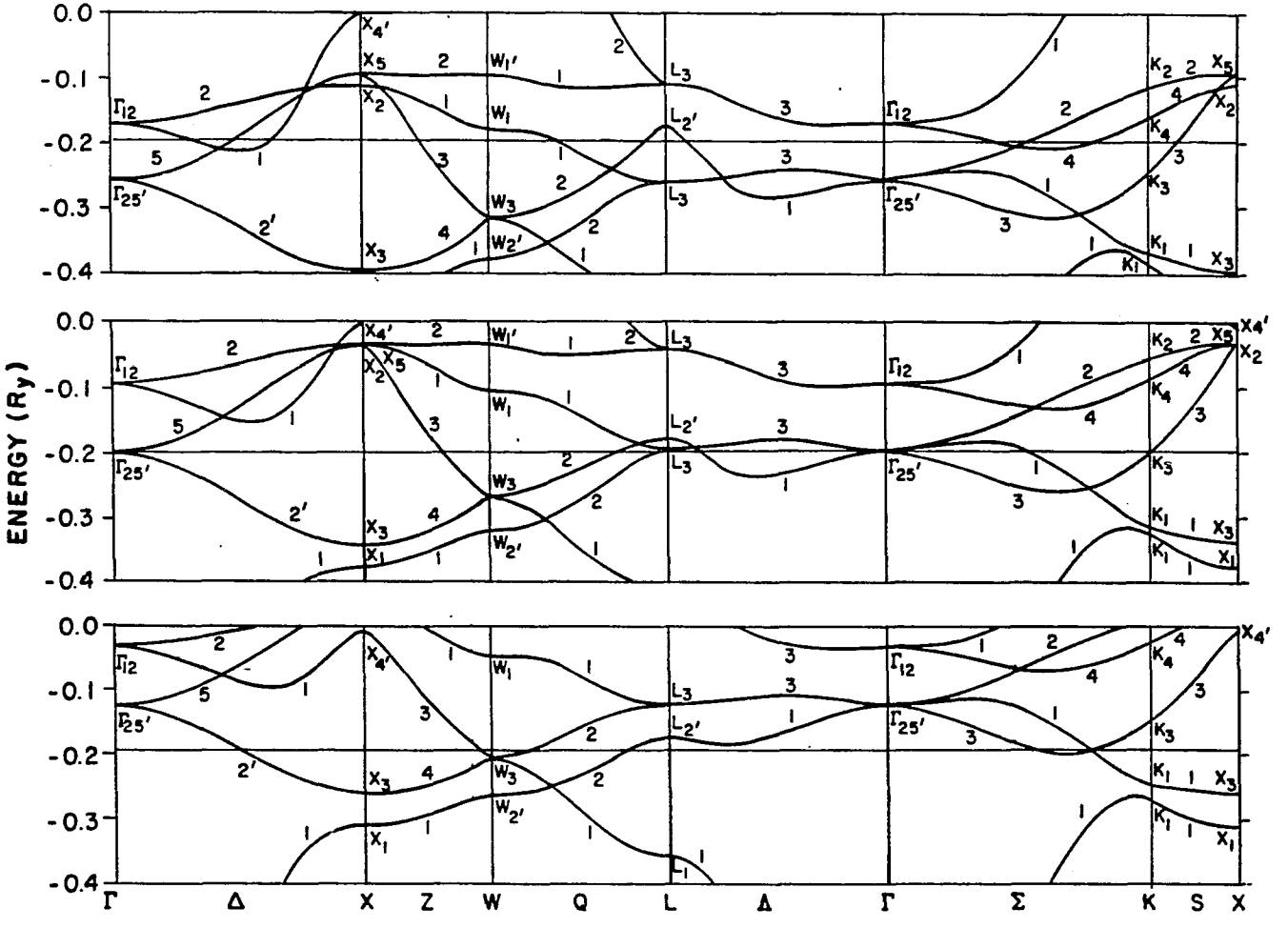

Figure 10. Minority-spin band structure of fcc Mn at lattice constants of 7.2 a.u. (top), 7.3 a.u. (middle), and 7.5 a.u. (bottom).

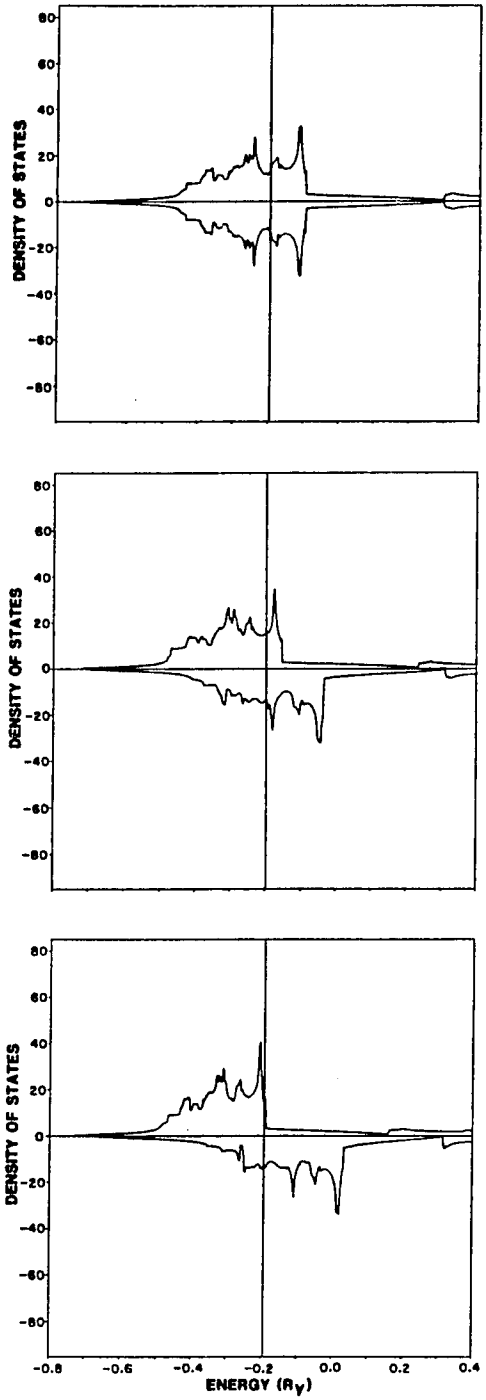

Figure 11. Density of states of fcc Mn (both spins) at lattice constants of 7.2 a.u. (top), 7.3 a.u. (middle), and 7.5 a.u. (bottom).

near the Γ_{12} point, which include some portions of the Λ_1, Σ_1, Σ_4, Δ_1, and Δ_2 majority-spin bands. The minority-spin density of states, on the other hand, presents a valley, located just below the Fermi level. To the left of that valley, there is a complex region, including a very sharp peak, centered at approximately -0.24 Ry, together with other smaller peaks. This complex region extends approximately down to -0.33 Ry and is composed of contributions from a number of bands around the points L_3, Γ_{25}', and K_3, including almost entirely the lower Λ_3 band and portions of Δ_1, Δ_5, Q_2 and
Q_1, Λ_1, Σ_3, Σ_1, and Σ_4.

The transition from the zero moment to the high moment region can then be described as follows. At a lattice constant of 7.2 a.u. the majority- and minority-spin bands are virtually identical, which is reflected in almost perfectly symmetrical curves for the up and down density of states.

When the lattice constant is increased from 7.2 to 7.3 a.u., the states corresponding to the smaller peaks of the majority-spin density are filled up, while at the same time, the states included in the sharp peak of the minority-spin density are emptied, producing the increase in the moment from 0 to $1.88\mu_B$. As the lattice constant continues to increase from 7.3 to 7.5 a.u., the large peak of the majority-spin density fills up, while more states are being emptied from the complex structure adjacent to the sharp peak of the minority-spin density. This causes the moment to increase to $3.42\mu_B$ at the end of the transition region. A further expansion of

the lattice should bring the remaining majority-spin states associated with the d-bands below the Fermi level, generating a more gradual increase in the moment.

We have discussed in detail the sharp transition from a non-magnetic to a high moment state. We cannot decide within the frame of our calculation what kind of magnetic ordering corresponds to each state. Preliminary susceptibility calculations by Zhao and coworkers[40] for fcc Mn at a = 6.8 a.u. indicate an antiferromagnetic ground state at that point. According to the calculations of Kübler,[8] fcc Mn is antiferromagnetic with alternating planes of up and down spins, parallel to the (001)-plane, in the whole range of lattice constants from a = 5.19 to 5.93 a.u.

The comparison with experimental results is complicated by the fact that the fcc phase occurs at high temperature, and it changes to face-centered tetragonal structure when quenched at room temperature.[15] In addition, several values of the magnetic moment are reported in the literature, corresponding to different antiferromagnetic alignments.[41] Again, a calculation of the total energy for different types of antiferromagnetic order would be useful in solving the problem of the ground state of fcc Mn. This kind of calculation is presently outside the scope of the program BNDPKG.

CHAPTER V

CONCLUSIONS

We have investigated the existence of different magnetic phases of bcc and fcc manganese by calculating the electronic band structure, magnetic moment, and density of states as a function of the lattice constant. This was motivated by the recent stabilization of new phases of manganese by epitaxial growth, in particular bcc manganese.[6]

For bcc manganese we considered a range of lattice constants from 5.2 to 8.0 a.u. We found that bcc manganese presents two magnetic phases: a low magnetic phase in which the moment is about 1 μ_B, and a high magnetic phase in which the moment varies from 2.4 up to 4.93 μ_B. There is a small region of lattice constants, between 5.9 and 6.025 a.u., in which both phases coexist. This corresponds to the existence of two local minima of the total energy, with different magnetic moments, but with the same lattice constant. At some point in the 'double-moment' region, there is an abrupt transition from the low moment to the high moment region. We were not able to determine the exact point of the transition since we did not perform a calculation of the total energy. Since the formalism of our band calculation does not allow for antiferromagnetism, it cannot identify the magnetic states as being either ferro- or antiferromagnetic. However, the susceptibility calculation of Fry and coworkers[10] at a = 5.397 a.u. indicates that the low moment state is ferromagnetic.

The results of our calculations can be compared with those of

Kübler[8] and Marcus and Moruzzi.[21] Thus, Fig. 12 shows the magnetic moment versus lattice constant curves according to this work (solid line), Marcus and Moruzzi (dashed line), and Kübler (dot-dashed line). Since Kübler considered ferromagnetic and antiferromagnetic states, both curves are shown, with a vertical line indicating the lattice constant at which the transition from a low moment ferromagnetic to a high moment antiferromagnetic state is expected to occur.

The three curves show a transition from a low moment to a high moment state. There is reasonable agreement in the values of the magnetic moment given by the three curves for the ferromagnetic state in the low moment region. Two of the curves (this work, and Marcus and Moruzzi) agree reasonably well on the lattice constant at which the transition is expected to occur. The value predicted by Kübler is smaller. In the high moment region this work and Marcus and Moruzzi agree reasonably well in the values of the magnetic moment for the ferromagnetic state. Kubler's curve for the antiferromagnetic state appears to agree with the other two, if extrapolated to larger lattice constants. Marcus and Moruzzi also found a region of zero magnetic moment at small lattice constants, which is outside the range of the other two curves. The bcc phase grown epitaxially by Arrott[6] showed no moment at a lattice constant of 5.4 a.u., in disagreement with all three calculations.

For fcc Mn we considered a range from 6.5 a.u. to 9.0 a.u. We found that fcc Mn presents two phases: a zero moment phase, and a high moment phase in which the moment varies from 1.88 μ_B up to 4.44 μ_B. There is a sharp transition from the zero moment to the

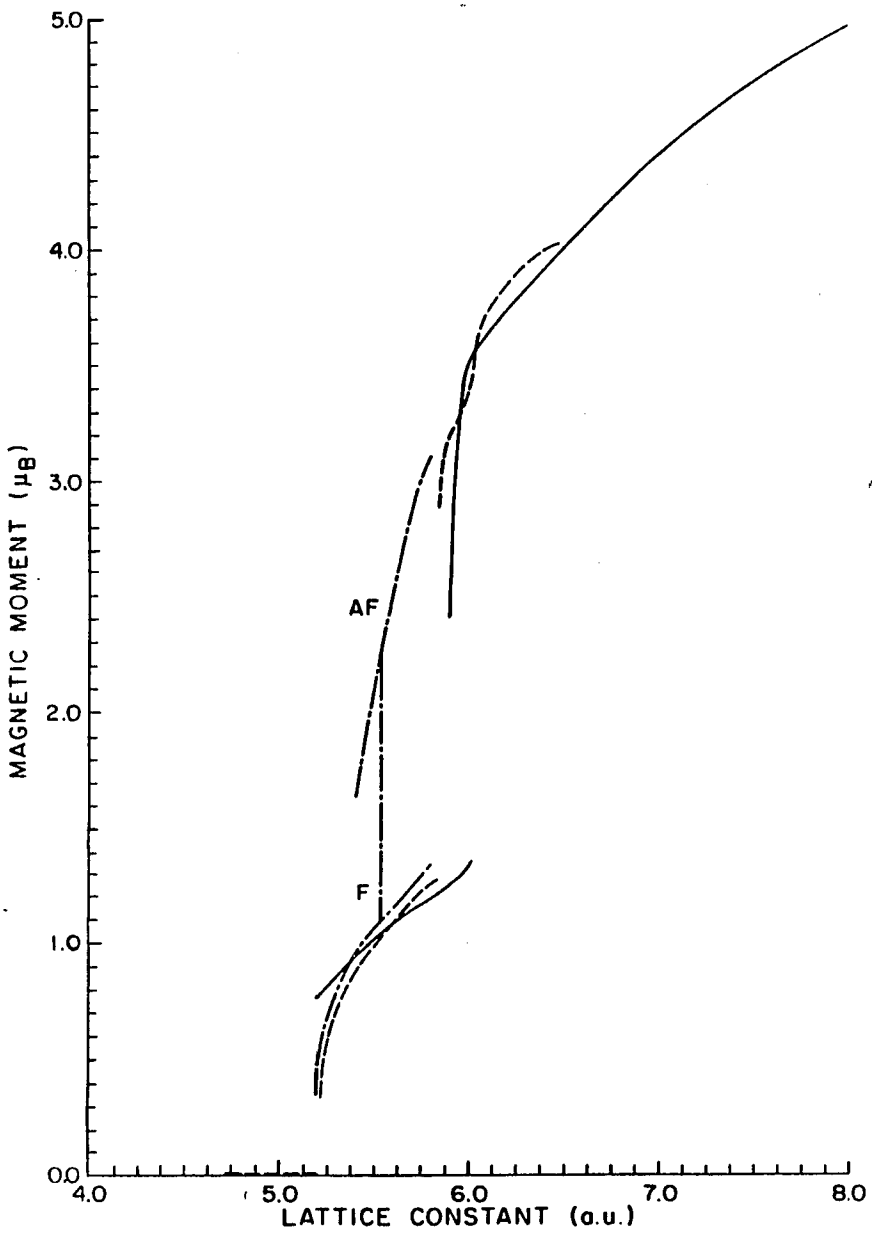

Fig. 12. Magnetic moment versus lattice constant for bcc Mn, according to this work (solid line), Marcus and Moruzzi[21] (dashed line) and Kübler[8] (dot-dashed line).

high moment state at a lattice constant of about a ≃ 7.275 a.u. No double-moment region was found in this case. The susceptibility calculations of Zhao et al.[40] for fcc Mn at a = 6.8 a.u. indicate an antiferromagnetic ground state at this point. Since, in general, a tendency toward antiferromagnetism is expected as the lattice constant increases,[48] the fact that the ground state is already antiferromagnetic at a = 6.8 a.u. indicates that it will probably remain antiferromagnetic as the lattice constant increases past this point. Thus we conclude that the ground state of fcc Mn is probably antiferromagnetic at all lattice constants > 6.8 a.u., including the region a > ~ 7.275 a.u., where the high-spin ferromagnetic moment was computed. Additional susceptibility calculations currently in progress are expected to confirm the fact that the ground state of fcc Mn is antiferromagnetic in the lattice constant range a > ~ 7.275 a.u.

The results of our calculations can be compared with those of Kübler.[8] (Marcus and Moruzzi did not consider fcc Mn). Figure 13 shows the magnetic moment versus lattice constant for fcc Mn, according to this work (solid line) and Kübler (dot-dashed line). Since Kübler considered ferromagnetic and antiferromagnetic phases, both curves are shown. Kübler's results for the total energy indicate that the ground state is antiferromagnetic for the whole range of lattice constants considered in his calculation. No phase transition is predicted in Kübler's calculations.

We were able to describe in detail the phase transitions for both bcc and fcc Mn in terms of the changes that occur in the band structure with the increase in the atomic volume. The mechanism

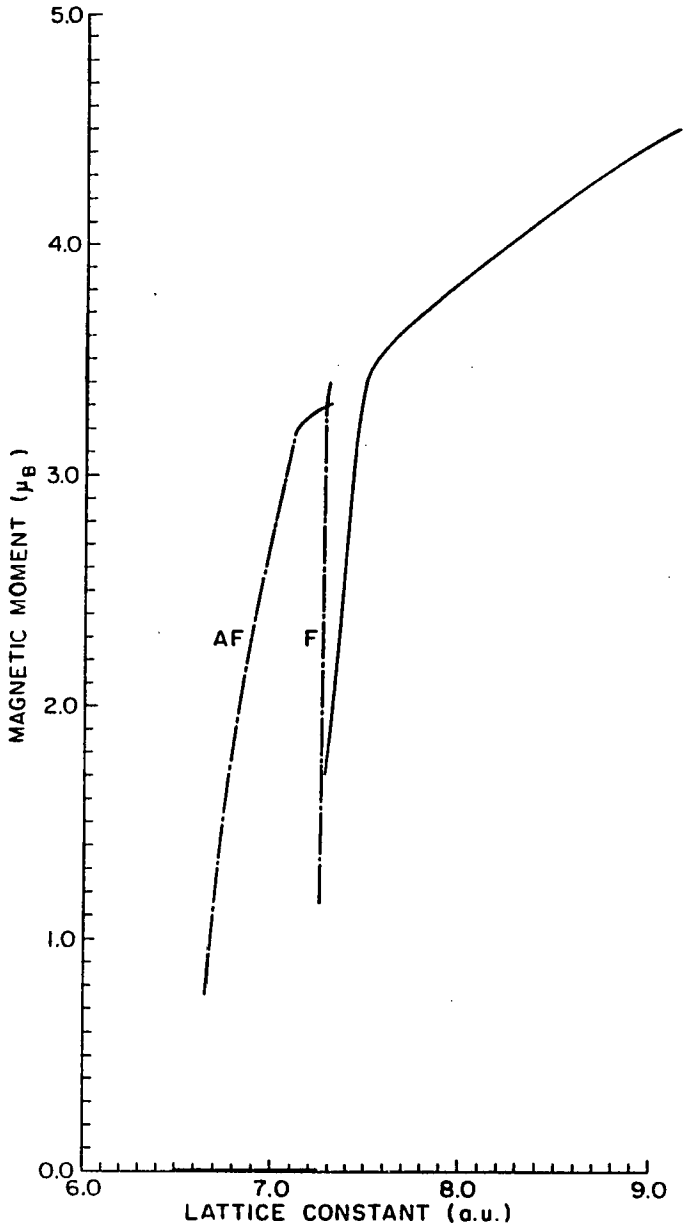

Fig. 13. Magnetic moment versus lattice constant for fcc Mn according to this work (solid line) and Kübler[8] (dot-dashed line).

operating is the same in both cases, namely the shifting of flat portions of the band structure across the Fermi surface, generating abrupt changes in the population of the majority- and minority-spin levels.

From the previous discussion we can make suggestions for future work.

From the experimental point of view, it would be very interesting to grow manganese on a variety of substrates with different interatomic distances, especially in the high moment region. Furthermore, other transition metals should be grown on a variety of substrates, so that we can eventually get a complete picture of the effect of the atomic volume on the magnetic structure of this group of metals.

It is evident from the discussions above that we have to extend our calculations in order to give a complete description of the magnetic structure of the transition metals. In the first place, a calculation of the total energy as a function of the lattice constant for the paramagnetic, ferromagnetic, and antiferromagnetic phase would indicate the most stable configuration at each lattice constant. To do this, the program BNDPKG would have to be extended to handle structures with more than one atom per unit cell, which is necessary for the inclusion of antiferromagnetic order in the formalism.

Finally, the fixed moment scheme of Moruzzi and coworkers[9] appears to be more suitable for the description of magnetic phases when more than one minima coexist. The implementation of this scheme in the formalism of BNDPKG seems to be the natural next step to take.

REFERENCES

1. R. J. Weiss and G. Mazzone, J. Appl. Cryst. 14, 401 (1981).
2. For a comparative study of the band structure of metals see, for example Refs. 3 and 4.
3. V. L. Moruzzi, J. F. Janak, and A. R. Williams, Calculated Electronic Properties of Metals, Pergamon Press, Inc. (1978).
4. D. Papaconstantopoulos, Handbook of the Band Structure of Elemental Solids, Plenum Press, New York (1986).
5. G. A. Prinz, Phys. Rev. Lett. 54, 1051 (1985).
6. A. S. Arrott, Bull. Am. Phys. Soc. 32, 707 (1987).
7. D. Bagayoko, and J. Callaway, Phys. Rev. B 28, 5419 (1983).
8. J. Kübler, in the Proceedings of the Institute von Laue-Langevin Workshop on 3d Metallic Magnetism, Grenoble, France, 1983, edited by D. Givord and K. Ziebeck (unpublished).
9. V. L. Moruzzi, P. M. Marcus, K. Schwarz and P. Mohn, Phys. Rev. B 34, 1784 (1986).
10. J. L. Fry, Y. Z. Zhao, N. E. Brener, G. Fuster and J. Callaway, Phys. Rev. B 36 868 (1987).
11. J. Madsen and O. K. Andersen in Magnetism and Magnetic Materials - 1975 (Philadelphia), Proceedings of the 21st Annual Conference on Magnetism and Magnetic Materials, edited by J. J. Becker, G. H. Lauder, and J. J. Rhyne (AIP, New York, 1976), p. 327.
12. J. Kübler, J. Magn. and Mag. Mater. 20, 107 (1980).
13. J. Kübler, J. Magn. and Mag. Mater. 20, 277 (1980).
14. J. Kübler, Phys. Lett. 81A, 81 (1981).

14. J. Kübler, Phys. Lett. 81A, 81 (1981).

15. A. M. Sully, Manganese, in 'Metallurgy of the Rarer Metals', edited by H. M. Finniston, Academic Press, New York (1955).

16. K. Sasaki, M. Betsuyaku, N. Mori, and T. Ukai, J. Magn. and Mag. Mater. 31-34, 41 (1983).

17. S. B. Shrivastava, and V. K. Ojha, Phys. Stat. Sol. b 121, 225 (1984).

18. G. C. Fletcher, J. Phys. F 1, 177 (1971).

19. S. Asano, and J. Yamashita, J. Phys. Soc. Jap. 31, 1000 (1971).

20. J. B. Goodenough, Phys. Rev. 120, 67 (1960).

21. P. M. Marcus and V. L. Moruzzi, to be published.

22. W. Kohn and L. J. Sham, Phys. Rev. A 140, 1133 (1965).

23. L. J. Sham and W. Khon, Phys. Rev. 145, 561 (1966).

24. P. Hohenberg and W. Khon, Phys. Rev. B 136, (1964).

25. J. Callaway, Quantum Theory of the Solid State, Academic Press, New York, (1976).

26. F. C. von der Lage and H. A. Bethe, Phys. Rev. 71, 612 (1947).

27. C. S. Wang and J. Callaway, Comput. Phys. Commun. 14, 327 (1978). The program BNDPKG is available from Comput., Phys. Commun. Program Library.

28. F. Bloch, Zeit Physik 52, 555 (1928).

29. U. von Barth and L. Hedin, J. Phys. C 5, 1629 (1972).

30. A. K. Rajagopal, S. P. Singhal and J. Kimball (unpublished), as quoted by A. K. Rajagopal, in 'Advances in Chemical Physics' edited by G. I. Prigogine and S. A. Rice, Wiley, New York, (1979).

31. J. Callaway and N. H. March, in Solid State Physics, edited by H. Ehrenreich, F. Seitz, and D. Turnbull, Academic Press, New York, (1984).

32. A. R. Williams and U. von Barth, Applications of Density Functional Theory to Atoms, Molecules and Solids, in 'Theory of the Inhomogeneous Electron Gas', edited by S. Lundqvist and N. H. March, Plenum, New York (1983).

33. E. E. Lafon and C. C. Lin, Phys. Rev. 152, 579 (1966).

34. S. F. Boys, Proc. Roy. Soc. (London), A200, 542 (1950).

35. I. Shavitt and M. Karplus, J. Chem. Phys. 36, 550 (1962).

36. R. C. Chaney and F. Dorman, Int. J. Quantum Chem. 8, 465 (1974).

37. A. J. H. Watchers, J. Chem. Phys. 52, 1033 (1970).

38. See Ref. 9, page 1786 and ff.

39. D. A. Papaconstantopoulos (private communication).

40. Y. Z. Zhao, J. L. Fry, P. C. Pattnaik, and K. Schwartzman (unpublished).

41. See for example, Ref. 1, p. 410.

42. H. Danan, A. Her, and A. J. P. Meyer, J. Appl. Phys. 39, 669 (1968).

43. D. Bagayoko, A. Ziegler, and J. Callaway, Phys. Rev. B 27, 7046 (1983).

44. A. R. Williams, J. Kübler, and C. D. Gelatt, Jr., Phys. Rev. B 19, 6094 (1979).

45. R. Walmsley, J. Thompson, D. Friedman, R. M. White, and T. H. Geballe, IEEE Trans. Magn. 19, 1992 (1983).

46. N. E. Brener, G. Fuster, J. Callaway, J. L. Fry, and Y. Z. Zhao, J. Appl. Phys. (to be published).

47. G. Fuster, N. E. Brener, J. Callaway, J. L. Fry, Y. Z. Zhao, and D. Papaconstantopoulos, Phys. Rev. B (to be published).

48. C. Herring, "Direct Exchange Between Well Separated Atoms", in "Magnetism", edited by G. Rado and H. Suhl (Academic Press, New York, 1966) Vol. 2B, p.1.

APPENDIX

Lattice constant = 5.2 a.u.; Fermi energy = 0.0011 Ry

Γ↑	Γ↓	P↑	P ↓
0.0010 (12)	0.0637 (12)	0.7408 (4)	0.7622 (4)
0.0010 (12)	0.0637 (12)	0.0269 (3)	0.0922 (3)
-0.1406 (25')	-0.0952 (25')	0.0269 (3)	0.0922 (3)
-0.1406 (25')	-0.0952 (25')	-0.2358 (4)	-0.2057 (4)
-0.1406 (25')	-0.0952 (25')	-0.2358 (4)	-0.2057 (4)
-0.6258 (1)	-0.6317 (1)	-0.2358 (4)	-0.2057 (4)

N↑	N↓	H↑	H↓
0.1293 (3)	0.1860 (3)	0.8004 (15)	0.8010 (15)
0.0568 (1')	0.0880 (4)	0.1015 (25')	0.1568 (25')
0.0230 (4)	0.0621 (1)	0.1015 (25')	0.1568 (25')
0.0031 (1)	0.0545 (1')	0.1015 (25')	0.1568 (25')
-0.2498 (2)	-0.2107 (2)	-0.3866 (12)	-0.3510 (12)
-0.3884 (1)	-0.3628 (1)	-0.3866 (12)	-0.3510 (12)

Table A.1.

Valence band energies at some symmetry points of the Brillouin zone of BCC manganese, in Rydbergs (Ry), for up (↑) and down (↓) spins.

Lattice constant = 5.8 a.u.; Fermi energy = -0.2077 Ry

Γ↑	Γ↓	P↑	P↓
-0.2134 (12)	-0.1177 (12)	0.3570 (4)	0.3880 (4)
-0.2134 (12)	-0.1177 (12)	-0.2012 (3)	-0.1036 (3)
-0.3013 (25')	-0.2324 (25')	-0.2012 (3)	-0.1036 (3)
-0.3013 (25')	-0.2324 (25')	-0.3658 (4)	-0.3174 (4)
-0.3013 (25')	-0.2324 (25')	-0.3658 (4)	-0.3174 (4)
-0.7183 (1)	-0.7188 (1)	-0.3658 (4)	-0.3174 (4)

N↑	N↓	H↑	H↓
-0.1340 (3)	-0.0518 (3)	0.4204 (15)	0.4237 (15)
-0.1613 (1')	-0.1056 (4)	-0.1508 (25')	-0.0700 (25')
-0.2030 (4)	-0.1248 (1)	-0.1508 (25')	-0.0700 (25')
-0.2142 (1)	-0.1624 (1')	-0.1508 (25')	-0.0700 (25')
-0.3648 (2)	-0.3023 (2)	-0.4380 (12)	-0.3707 (12)
-0.4684 (1)	-0.4258 (1)	-0.4380 (12)	-0.3707 (12)

Table A.2.

Valence band energies at some symmetry points of the Brillouin zone of BCC manganese, in Rydbergs (Ry), for up (↑) and down (↓) spins.

Lattice constant = 5.925 a.u.; Fermi energy = -0.2358 Ry

Γ↑	Γ↓	P↑	P↓
-0.2419 (12)	-0.1397 (12)	0.3018 (4)	0.3342 (4)
-0.2419 (12)	-0.1397 (12)	-0.2317 (3)	-0.1278 (3)
-0.3216 (25')	-0.2482 (25')	-0.2317 (3)	-0.1278 (3)
-0.3216 (25')	-0.2482 (25')	-0.3808 (3)	-0.3288 (3)
-0.3216 (25')	-0.2482 (25')	-0.3808 (4)	-0.3288 (4)
-0.7240 (1)	-0.7239 (1)	-0.3808 (4)	-0.3288 (4)

N↑	N↓	H↑	H↓
-0.1692 (3)	-0.0825 (3)	0.3650 (15)	0.3688 (15)
-0.1882 (1')	-0.1294 (4)	-0.1844 (25')	-0.0991 (25')
-0.2332 (4)	-0.1474 (1)	-0.1844 (25')	-0.0991 (25')
-0.2429 (1)	-0.1890 (1')	-0.1844 (25')	-0.0991 (25')
-0.3780 (2)	-0.3108 (2)	-0.4397 (12)	-0.3646 (12)
-0.4758 (1)	-0.4297 (1)	-0.4397 (12)	-0.3646 (12)

Table A.3.

Valence band energies at some symmetry points of the Brillouin zone of BCC manganese, in Rydbergs (Ry), for up (↑) and down (↓) spins. (Low moment state).

Lattice constant = 5.95 a.u.; Fermi energy = -0.1989 Ry

Γ↑	Γ↓	P↑	P↓
-0.2406 (12)	-0.0363 (12)	0.2912 (4)	0.4017 (4)
-0.2406 (12)	-0.0363 (12)	-0.2306 (3)	-0.0230 (3)
-0.3258 (25')	-0.1418 (25')	-0.2306 (3)	-0.0230 (3)
-0.3258 (25')	-0.1418 (25')	-0.3850 (4)	-0.2450 (4)
-0.3258 (25')	-0.1418 (25')	-0.3850 (4)	-0.2450 (4)
-0.7291 (1)	-0.6811 (1)	-0.3850 (4)	-0.2450 (4)

N↑	N↓	H↑	H↓
-0.1742 (3)	0.0336 (3)	0.3494 (15)	0.4095 (15)
-0.1963 (1')	-0.0247 (4)	-0.1893 (25')	0.0160 (25')
-0.2321 (4)	-0.0421 (1)	-0.1893 (25')	0.0160 (25')
-0.2435 (1)	-0.1509 (1')	-0.1893 (25')	0.0160 (25')
-0.3816 (2)	-0.2089 (2)	-0.4364 (12)	-0.2767 (12)
-0.4784 (1)	-0.3543 (1)	-0.4364 (12)	-0.2767 (12)

Table A.4.

Valence band energies at some symmetry points of the Brillouin zone of BCC manganese, in Rydberg (Ry), for up (↑) and down (↓) spins. (High moment state).

Lattice constant = 6.0 a.u.; Fermi energy = -0.1941 Ry

Γ↑	Γ↓	P↑	P↓
-0.2462 (12)	-0.0263 (12)	0.2714 (4)	0.3967 (4)
-0.2462 (12)	-0.0263 (12)	-0.2369 (3)	-0.0136 (3)
-0.3318 (25')	-0.1269 (25')	-0.2369 (3)	-0.0136 (3)
-0.3318 (25')	-0.1269 (25')	-0.3896 (4)	-0.2333 (4)
-0.3318 (25')	-0.1269 (25')	-0.3896 (4)	-0.2333 (4)
-0.7314 (1)	-0.6743 (1)	-0.3896 (4)	-0.2333 (4)

N↑	N↓	H↑	H↓
-0.1850 (3)	0.0452 (3)	0.3284 (15)	0.3988 (15)
-0.2065 (1')	-0.0153 (4)	-0.1996 (25')	0.0279 (25')
-0.2382 (4)	-0.0314 (1)	-0.1996 (25')	0.0279 (25')
-0.2500 (1)	-0.1524 (1')	-0.1996 (25')	0.0279 (25')
-0.3851 (2)	-0.1921 (2)	-0.4334 (12)	-0.2585 (12)
-0.4800 (1)	-0.3419 (1)	-0.4334 (12)	-0.2585 (12)

Table A.5.

Valence band energies at some symmetry points of the Brillouin zone of BCC manganese, in Rydbergs (Ry), for up (↑) and down (↓) spins. (High moment state).

Lattice constant = 8.0 a.u.; Fermi energy = 0.2647

Γ↑	Γ↓	P↑	P↓
-0.4924 (12)	-0.1894 (12)	0.2416 (4)	0.1323 (4)
-0.4924 (12)	-0.1894 (12)	-0.4940 (3)	-0.1915 (3)
-0.5033 (25')	-0.2094 (25')	-0.4940 (3)	-0.1915 (3)
-0.5033 (25')	-0.2094 (25')	-0.5166 (4)	-0.2673 (4)
-0.5033 (25')	-0.2094 (25')	-0.5166 (4)	-0.2673 (4)
-0.6719 (1)	-0.6026 (1)	-0.5166 (4)	-0.2673 (4)

N↑	N↓	H↑	H↓
-0.3356 (1')	-0.1818 (3)	-0.0769 (15)	-0.0056 (15)
-0.4820 (3)	-0.1915 (4)	-0.4838 (25')	-0.1841 (25')
-0.4937 (1)	-0.1921 (1)	-0.4838 (25')	-0.1841 (25')
-0.4940 (4)	-0.2131 (2)	-0.4838 (25')	-0.1841 (25')
-0.5061 (2)	-0.2812 (1')	-0.5027 (12)	-0.2027 (12)
-0.5293 (1)	-0.3209 (1)	-0.5027 (12)	-0.2027 (12)

Table A.6.

Valence band energies at some symmetry points of the Brillouin zone of BCC manganese, in Rydbergs (Ry), for up (↑) and down (↓) spins.

Lattice constant = 7.0 a.u.; Fermi energy = -0.1536 Ry

Γ↑	Γ↓	X↑	X↓	W↑	W↓
-0.1239 (12)	-0.1236 (12)	0.0607 (4')	0.0606 (4')	0.4646 (3)	0.4646 (3)
-0.1239 (12)	-0.1236 (12)	-0.0382 (5)	-0.0380 (5)	-0.0381 (1')	-0.0379 (1')
-0.2227 (25')	-0.2226 (25')	-0.0382 (5)	-0.0380 (5)	-0.1339 (1)	-0.1337 (1)
-0.2227 (25')	-0.2226 (25')	-0.0577 (2)	-0.0574 (2)	-0.2872 (3)	-0.2872 (3)
-0.2227 (25')	-0.2226 (25')	-0.3825 (3)	-0.3824 (3)	-0.2872 (3)	-0.2872 (3)
-0.7012 (1)	-0.7013 (1)	-0.4272 (1)	-0.4271 (1)	-0.3609 (2')	-0.3608 (2')

L↑	L↓	K↑	K↓
-0.0557 (3)	-0.0555 (3)	0.3331 (3)	0.3331 (3)
-0.0557 (3)	-0.0555 (3)	-0.0626 (2)	-0.0624 (2)
-0.1296 (2')	-0.1297 (2')	-0.1121 (4)	-0.1119 (4)
-0.2277 (3)	-0.2276 (3)	-0.2056 (3)	-0.2055 (3)
-0.2277 (3)	-0.2276 (3)	-0.3454 (1)	-0.3453 (1)
-0.4335 (1)	-0.4335 (1)	-0.3704 (1)	-0.3703 (1)

Table A.7.

Valence bands energies at some symmetry points of the Brillouin zone of FCC manganese in Rydbergs (Ry), for up (↑) and down (↓) spins.

Lattice constant = 7.2 a.u.; Fermi energy = -0.1950 Ry

Γ↑	Γ↓	X↑	X↓	W↑	W↓
-0.1691 (12)	-0.1687 (12)	0.0017 (4')	0.0017 (4')	0.3763 (3)	0.3763 (3)
-0.1691 (12)	-0.1687 (12)	-0.0939 (5)	-0.0937 (5)	-0.0938 (1')	-0.0936 (1')
-0.2567 (25')	-0.2565 925')	-0.0939 (5)	-0.0937 (5)	-0.1774 (1)	-0.1770 (1)
-0.2567 (25')	-0.2565 (25')	-0.1106 (2)	-0.1102 (2)	-0.3151 (3)	-0.3150 (3)
-0.2567 (25')	-0.2565 (25')	-0.3967 (3)	-0.3966 (3)	-0.3151 (3)	-0.3150 (3)
-0.7172 (1)	-0.7172 (1)	-0.4362 (1)	-0.4360 (1)	-0.3788 (2')	-0.3786 (2')

L↑	L↓	K↑	K↓
-0.1092 (3)	-0.1088 (3)	0.2518 (3)	0.2519 (3)
-0.1092 (3)	-0.1088 (3)	-0.1152 (3)	-0.1150 (2)
-0.1743 (2')	-0.1743 (2')	-0.1583 (4)	-0.1579 (4)
-0.2602 (3)	-0.2599 (3)	-0.2432 (3)	-0.2430 (3)
-0.2602 (3)	-0.2599 (3)	-0.3667 (1)	-0.3666 (1)
-0.4509 (1)	-0.4508 (1)	-0.3856 (1)	-0.3854 (1)

Table A.8.

Valence bands energies at some symmetry points of the Brillouin zone of FCC manganese in Rydbery (Ry), for up (↑) and down (↓) spins.

Lattice constant = 7.3 a.u.; Fermi energy = - 0.1969 Ry

Γ↑	Γ↓	X↑	X↓	W↑	W↓
-0.2372 (12)	-0.0929 (12)	-0.0278 (4')	-0.0061 (4')	0.3247 (3)	0.3766 (3)
-0.2372 (12	-0.0929 (12)	-0.1523 (5)	-0.0336 (5)	-0.1522 (1')	-0.0335 (1')
-0.3013 (25')	-0.1975 (25')	-0.1523 (5)	-0.0336 (5)	-0.2426 (1)	-0.1048 (1)
-0.3013 (25')	-0.1975 (25')	-0.1843 (2)	-0.0336 (2)	-0.3513 (3)	-0.2673 (3)
-0.3013 (25')	-0.1975 (25')	-0.4276 (3)	-0.3399 (3)	-0.3513 (3)	-0.2673 (3)
-0.7263 (1)	-0.7057 (1)	-0.4709 (1)	-0.3758 (1)	-0.4187 (2')	-0.3209 (2')

L↑	L↓	K↑	K↓
-0.1726 (3)	-0.0417 (3)	0.2023 (3)	0.2596 (3)
-0.1726 (3)	-0.0417 (3)	-0.1717 (2)	-0.0549 (2)
-0.1958 (2')	-0.1765 (2')	-0.2262 (4)	-0.0841 (4)
-0.3128 (3)	-0.1927 (3)	-0.2835 (3)	-0.2005 (3)
-0.3128 (3)	-0.1927 (3)	-0.3993 (1)	-0.3169 (1)
-0.4766 (1)	-0.4113 (1)	-0.4248 (1)	-0.3256 (1)

Table A.9.

Valence bands energies at some symmetry points of the Brillouin zone of FCC manganese in Rydberg (Ry), for up (↑) and down (↓) spins.

Lattice constant = 7.5 a.u.; Fermi energy = -0.1969 Ry

Γ↑	Γ↓	X↑	X↓	W↑	W↓
-0.2560 (12)	-0.0331 (12)	-0.0728 (4')	-0.0338 (5)	0.2567 (3)	0.3713 (3)
-0.2560 (12)	-0.0331 (12)	-0.1882 (5)	-0.0338 (5)	-0.1882 (1')	-0.0338 (1')
-0.3216 (25')	-0.1234 (25')	-0.1882 (5)	-0.0233 (5)	-0.2608 (1)	-0.0472 (1)
-0.3216 (25')	-0.1234 (25')	-0.2082 (2)	-0.0102 (2)	-0.3677 (3)	-0.2047 (3)
-0.3216 (25')	-0.1234 (25')	-0.4327 (3)	-0.2586 (3)	-0.3677 (3)	-0.2047 (3)
-0.7347 (1)	-0.6760 (1)	-0.4665 (1)	-0.3105 (1)	-0.4211 (2')	-0.2641 (2')

L↑	L↓	K↑	K↓
-0.2031 (3)	0.0214 (3)	0.1410 (3)	0.2673 (3)
-0.2031 (3)	-0.0214 (3)	-0.2054 (2)	0.0136 (2)
-0.2280 (2')	-0.1235 (3)	-0.2461 (4)	-0.0265 (4)
-0.3264 (3)	-0.1235 (3)	-0.3074 (3)	-0.1490 (3)
-0.3264 (3)	-0.1732 (2')	-0.4104 (1)	-0.2452 (1)
-0.4859 (1)	-0.3544 (1)	-0.4252 (1)	-0.2682 (1)

Table A. 10.

Valence bands energies at some symmetry points of the Brillouin zone of FCC manganese in Rydbergs (Ry), for up (↑) and down (↓) spins.

VITA

The author was born on January 16, 1951, in Los Andes, Chile. He received his B.S. degree in engineering from Universidad Catolica, Valparaiso, Chile in 1978. He taught in Universidad Santa Maria, Valparaíso, Chile until 1980. He enrolled in Louisiana State University in 1981, where he received his M.S. degree in Physics in 1985. He has worked on the calculation of electronic band structures of transition metals under Professor J. Callaway.

DOCTORAL EXAMINATION AND DISSERTATION REPORT

Candidate: Gonzalo Fuster

Major Field: Physics

Title of Dissertation: Magnetism in BCC and FCC Manganese

Approved:

Major Professor and Chairman

Dean of the Graduate School

EXAMINING COMMITTEE:

Date of Examination:

November 20, 1987